Physica D 326 (2016) 1–20

Contents lists available at ScienceDirect

Physica D

journal homepage: www.elsevier.com/locate/physd

Existence and stability of $\mathcal{PT}$-symmetric states in nonlinear two-dimensional square lattices

Haitao Xu [a,*], P.G. Kevrekidis [a], Dmitry E. Pelinovsky [b,c]

[a] Department of Mathematics and Statistics, University of Massachusetts, Amherst, MA 01003-9305, USA
[b] Department of Mathematics and Statistics, McMaster University, Hamilton, Ontario, Canada, L8S 4K1
[c] Department of Applied Mathematics, Nizhny Novgorod State Technical University, Nizhny Novgorod, Russia

HIGHLIGHTS

- We present a study on stationary states in PT-symmetric lattice settings in the weak coupling limit.
- We report the existence and stability properties of PT-symmetric soliton and vortex configurations.
- All examined vortex configurations are unstable with respect to small perturbations.
- One branch of solutions extending soliton configurations is spectrally stable.
- This offers an analytical perspective to this topic and corroborates results by numerical results.

ARTICLE INFO

Article history:
Received 5 November 2015
Accepted 26 March 2016
Available online 2 April 2016
Communicated by V.M. Perez-Garcia

Keywords:
PT-symmetry
2D square lattice
Discrete soliton
Discrete vortex
Anti-continuum limit
dNLS

ABSTRACT

Solitons and vortices symmetric with respect to simultaneous parity ($\mathcal{P}$) and time reversing ($\mathcal{T}$) transformations are considered on the square lattice in the framework of the discrete nonlinear Schrödinger equation. The existence and stability of such $\mathcal{PT}$-symmetric configurations is analyzed in the limit of weak coupling between the lattice sites, when predictions on the elementary cell of a square lattice (i.e., a single square) can be extended to a large (yet finite) array of lattice cells. In particular, we find all examined vortex configurations are unstable with respect to small perturbations while a branch extending soliton configurations is spectrally stable. Our analytical predictions are found to be in good agreement with numerical computations.

1. Introduction

Networks of coupled nonlinear oscillators with balanced gains and losses have been considered recently in the context of nonlinear $\mathcal{PT}$-symmetric lattices. Among many other questions, attention has been paid to issues of linear and nonlinear stability of constant equilibrium states [1] and spatially distributed steady states [2,3] in such systems. More generally, the study of solitary waves in such $\mathcal{PT}$-symmetric lattices [4] has garnered considerable attention over the years, as can be inferred also from a recent comprehensive review on the subject [5]. A significant recent boost to the relevant interest has been offered by the experimental observation of optical solitons in lattice settings [6]. Many of the relevant theoretical notions have been developed also in continuum systems with periodic potentials in both scalar [7,8] and vector [9] settings.

In higher dimensions, the number of studies of $\mathcal{PT}$-symmetric lattices and the coherent structures that they support is considerably more limited. Nonlinear states bifurcating out of linear (point spectrum) modes of a potential and their stability have been studied [10] and so have gap solitons [11]. However, an understanding of fundamentally topological states such as vortices and their existence and stability properties is still an active theme of study [12]. The few studies addressing these topological structures have been chiefly numerical in nature [13–15]. It is, thus, the aim of the present study to explore a two-dimensional square lattice setting and to provide an understanding of the existence and stability properties of the stationary states it can support, placing a particular emphasis on the vortical structures.

We will be particularly interested in the following $\mathcal{PT}$-symmetric model of the discrete nonlinear Schrödinger (dNLS)

* Corresponding author.
E-mail addresses: haitao@math.umass.edu (H. Xu), kevrekid@gmail.com (P.G. Kevrekidis), dmpeli@math.mcmaster.ca (D.E. Pelinovsky).

http://dx.doi.org/10.1016/j.physd.2016.03.014
0167-2789/

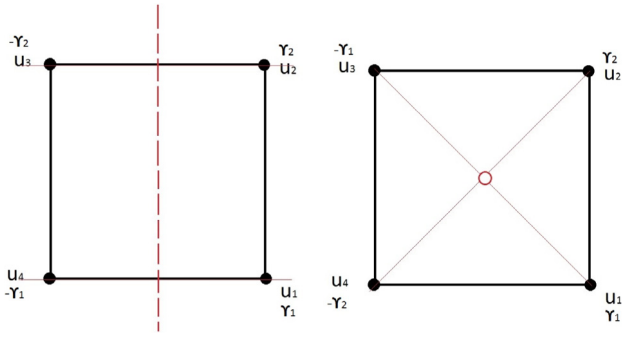

Fig. 1. Schematic $\mathcal{PT}$-symmetry for the elementary cell of the square lattice.

type [16],

$$i\frac{d\psi_{j,k}}{dt} + (\Delta\psi)_{j,k} + |\psi_{j,k}|^2\psi_{j,k} = i\gamma_{j,k}\psi_{j,k}, \tag{1}$$

where $\psi_{j,k} \in \mathbb{C}$ depends on the lattice site $(j, k) \in \mathbb{Z}^2$ and the time variable $t \in \mathbb{R}$ (in optics, this corresponds to the spatial propagation direction), $(\Delta\psi)_{j,k}$ denotes the discrete Laplacian operator at the (j, k) site of the square lattice, and the distribution of the parameter values $\gamma_{j,k} \in \mathbb{R}$ for gains or losses is supposed to be $\mathcal{PT}$-symmetric. The dNLS equation is a prototypical model for the study of optical waveguide arrays [17], and the principal setting in which $\mathcal{PT}$-symmetry was first developed experimentally (in the context of few waveguides, such as the dimer setting [18]).

The $\mathcal{PT}$-symmetry holds if the distribution of $\gamma_{j,k}$ is odd with respect to reflections of the lattice sites in $\mathbb{Z}^2$ about a selected center or line of symmetry. In particular, we will consider two natural symmetric configurations in the elementary cell, as shown in Fig. 1. The left panel shows the symmetry about a vertical line located on the equal distance between two vertical arrays of lattice sites. The right panel shows the symmetry about a center point in the elementary cell of the square lattice.

Assuming every cell of the lattice preserves the same type of symmetry, we will study two types of gain–loss structures of the square lattices as illustrated in the top row of Fig. 2. In addition, we consider the special situations where two types of symmetries hold simultaneously. In the bottom left panel of Fig. 2, the square lattice is equipped with symmetries about both vertical and horizontal lines, which corresponds to $\gamma_2 = -\gamma_1$ on the left panel of Fig. 1. The bottom right panel of Fig. 2 describes the situation where symmetry about the horizontal line and symmetry about the center of each cell both come into play, which corresponds to $\gamma_2 = -\gamma_1$ on the right panel of Fig. 1.

In order to enable the analytical consideration of the existence and stability of vortices in the $\mathcal{PT}$-symmetric dNLS equation (1), we will consider steady states in the limit of large energy [2,3,19]. This enables a formalism of the so-called anti-continuum limit in the analysis of steady states in nonlinear lattices [20]. In particular, we set $\psi_{j,k}(t) = \varphi_{j,k}(t)e^{iEt}$ and introduce the scaling

$$E = \epsilon^{-1}, \qquad \varphi_{j,k}(t) = u_{j,k}(\tau)\epsilon^{-1/2}, \quad \tau = t\epsilon^{-1}. \tag{2}$$

As a result of this transformation, the $\mathcal{PT}$-symmetric dNLS equation (1) can be rewritten in the equivalent form

$$i\frac{du_{j,k}}{d\tau} - u_{j,k} + \epsilon(\Delta u)_{j,k} + |u_{j,k}|^2u_{j,k} = i\epsilon\gamma_{j,k}u_{j,k}, \tag{3}$$

where the parameter ϵ is small in the limit of large energy E. Moreover, if $\epsilon \to 0^+$, then $E \to +\infty$, whereas if $\epsilon \to 0^-$, then $E \to -\infty$. Setting $\epsilon = 0$ yields the system of uncoupled conservative nonlinear oscillators, therefore, small values of ϵ can be considered by the perturbation theory from the uncoupled conservative limit. In light of this transformation, the analysis will follow our previous work on existence and stability of vortices in conservative lattices of the dNLS type [21] (see also applications in [22,23]). In what follows, we apply the continuation technique to obtain definite conclusions on vortices in the $\mathcal{PT}$-symmetric dNLS equation (3).

We will focus on the basic vortex configuration, for which the excited oscillators are only supported on the elementary cell shown in Fig. 1. In this case, the definite conclusions on existence of $\mathcal{PT}$-symmetric vortices can already be extracted from studies of the $\mathcal{PT}$-symmetric dNLS equation (3) on four sites only, see Section 2. This is the so-called plaquette setting in [15]. With the $\mathcal{PT}$-symmetry in hand and appropriate (e.g. Dirichlet) boundary conditions on the square lattice truncated symmetrically in a suitable square domain, one can easily upgrade these conclusions for the full dNLS equation (3), see Section 3. The existence results remain valid in the infinite square lattice, thanks to the choice of the sequence spaces such as $\ell^2(\mathbb{Z}^2)$.

Stability of $\mathcal{PT}$-symmetric vortices on the four sites can be analyzed in the framework of the Lyapunov–Schmidt reduction method, see Section 4. However, one needs to be more careful to study stability of the localized steady states on large square lattices because the zero equilibrium may become spectrally unstable in the lattices with spatially extended gains and losses [19,24]. Stable configurations depend sensitively on the way gains and losses compensate each other, especially if the two-dimensional square lattice is truncated to a finite size. These aspects are discussed in Section 5 for both the zero equilibrium and the soliton/vortex patterns. Finally, Section 6 provides some conclusions, as well as offers an outlook towards future work.

2. Existence of $\mathcal{PT}$-symmetric vortices in the elementary cell

Let us consider the elementary cell of the square lattice shown in Fig. 1. We will enumerate the four corner sites in the counterclockwise order with the first site to lie at the bottom right. By the construction, the configuration has a cyclic symmetry with respect to the shift along the elementary cell.

Looking for the steady-state solutions $u_j(\tau) = \phi_j e^{-2i\epsilon\tau}$, where the exponential factor removes the diagonal part of the Laplacian operator Δ connecting each of the three lattice sites in the elementary cell, we rewrite the $\mathcal{PT}$-symmetric dNLS equation (3) in the explicit form

$$\begin{cases} (1-|\phi_1|^2)\phi_1 - \epsilon(\phi_2+\phi_4 - i\gamma_1\phi_1) = 0, \\ (1-|\phi_2|^2)\phi_2 - \epsilon(\phi_1+\phi_3 - i\gamma_2\phi_2) = 0, \\ (1-|\phi_3|^2)\phi_3 - \epsilon(\phi_2+\phi_4 - i\gamma_3\phi_3) = 0, \\ (1-|\phi_4|^2)\phi_4 - \epsilon(\phi_1+\phi_3 - i\gamma_4\phi_4) = 0. \end{cases} \tag{4}$$

In the following, we consider two types of $\mathcal{PT}$-symmetric configurations for the gain and loss parameters. These two configurations correspond to the two panels of Fig. 1.

(S1) Symmetry about the vertical line: $\gamma_1 = -\gamma_4$ and $\gamma_2 = -\gamma_3$;
(S2) Symmetry about the center: $\gamma_1 = -\gamma_3$ and $\gamma_2 = -\gamma_4$.

Besides the cyclic symmetry, one can also flip each of the two configurations (S1) and (S2) about the vertical or horizontal axes of symmetries. In addition, for the configuration shown on the right panel of Fig. 1, one can also flip the configuration about the center of symmetry, either between the first and third sites or between the second and fourth sites.

The $\mathcal{PT}$-symmetric stationary states that we explore correspond to particular reductions of the system of algebraic equations (4), namely,

(S1) Symmetry about the vertical line: $\phi_1 = \bar{\phi}_4$ and $\phi_2 = \bar{\phi}_3$;
(S2) Symmetry about the center: $\phi_1 = \bar{\phi}_3$ and $\phi_2 = \bar{\phi}_4$.

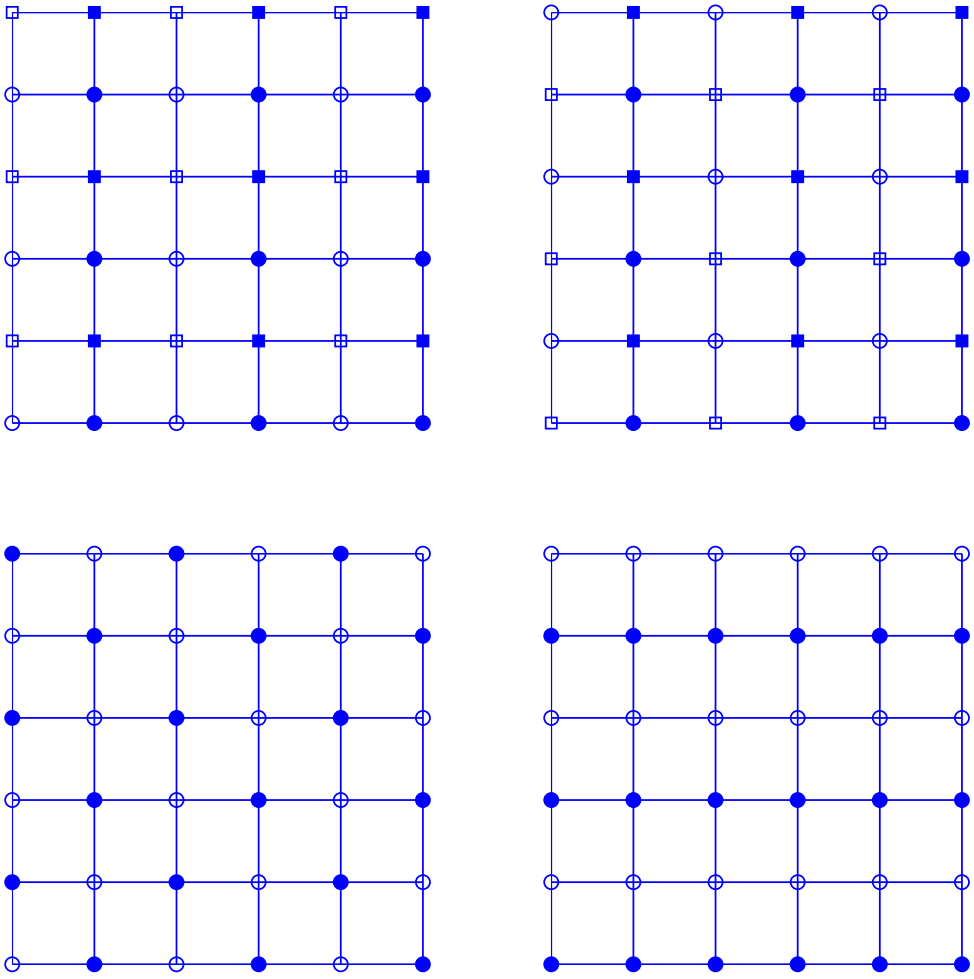

Fig. 2. Top row: gain and loss structures in the square lattice that correspond to the symmetric configurations in Fig. 1. Solid circle: γ_1; hollow circle: $-\gamma_1$; solid square: γ_2; hollow square: $-\gamma_2$. Bottom row: highly symmetric situations where two types of symmetries hold at the same time with $\gamma_2 = -\gamma_1$.

Due to the symmetry conditions, the system of algebraic equation (4) reduces to two equations for ϕ_1 and ϕ_2 only. We shall classify all possible solutions separately for the two different symmetries. We also note the symmetry of solutions with respect to changes in the sign of $\{\phi_j\}_{1\le j\le 4}$, $\{\gamma_j\}_{1\le j\le 4}$, and ϵ.

Remark 2.1. If $\{\phi_j\}_{1\le j\le 4}$ solves the system (4) with $\{\gamma_j\}_{1\le j\le 4}$ and ϵ, then $\{\overline{\phi}_j\}_{1\le j\le 4}$ solves the same system with $\{-\gamma_j\}_{1\le j\le 4}$ and ϵ.

Remark 2.2. If $\{\phi_j\}_{1\le j\le 4}$ solves the system (4) with $\{\gamma_j\}_{1\le j\le 4}$ and ϵ, then $\{(-1)^j\overline{\phi}_j\}_{1\le j\le 4}$ solves the same system with $\{\gamma_j\}_{1\le j\le 4}$ and $-\epsilon$.

Remark 2.3. If $\{\phi_j\}_{1\le j\le 4}$ solves the system (4) with $\{\gamma_j\}_{1\le j\le 4}$ and ϵ, then $\{-\phi_j\}_{1\le j\le 4}$ solves the same system with $\{\gamma_j\}_{1\le j\le 4}$ and ϵ.

As is known from the previous work [21], if gains and losses are absent, that is, if $\gamma_j = 0$ for all j, then the solutions of the system (4) are classified into two groups:

- discrete solitons if $\arg(\phi_j) = \theta_0 \mod(\pi)$ for all j;
- discrete vortices, otherwise.

Persistence of discrete solitons is well known for the $\mathcal{PT}$-symmetric networks [2,3,19], whereas persistence of discrete vortices has not been theoretically established in the literature. The term "persistence" refers to the unique continuation of the limiting configuration at $\epsilon = 0$ with respect to the small parameter ϵ. The gain and loss parameters are considered to be fixed in this continuation.

2.1. Symmetry about the vertical line (S1)

Under conditions $\gamma_1 = -\gamma_4$, $\gamma_2 = -\gamma_3$, $\phi_1 = \bar{\phi}_4$, and $\phi_2 = \bar{\phi}_3$, the system (4) reduces to two algebraic equations:

$$\begin{cases} f_1 := (1 - |\phi_1|^2)\phi_1 - \epsilon(\bar{\phi}_1 + \phi_2 - i\gamma_1\phi_1) = 0, \\ f_2 := (1 - |\phi_2|^2)\phi_2 - \epsilon(\bar{\phi}_2 + \phi_1 - i\gamma_2\phi_2) = 0. \end{cases} \tag{5}$$

In general, it is not easy to solve the system (5) for any given γ_1, γ_2 and ϵ. However, branches of solutions can be classified through continuation from the limiting case $\epsilon = 0$ to an open set $\mathcal{O}(0)$ of the ϵ values that contains 0. Simplifying the general approach described in [21] for the $\mathcal{PT}$-symmetric vortex configurations, we obtain the following result.

Lemma 2.1. *Consider the general solution of the system (5) at $\epsilon = 0$ in the form:*

$$\phi_j^{(\epsilon=0)}(\theta_j) = e^{i\theta_j}, \quad \theta_j \in \mathbb{T} := \mathbb{R}/(2\pi\mathbb{Z}). \tag{6}$$

For every γ_1 and γ_2, there exists a C^∞ function $\boldsymbol{h}(\boldsymbol{\theta}, \epsilon) : \mathbb{T}^2 \times \mathbb{R} \to \mathbb{R}^2$ such that there exists a unique solution $\boldsymbol{\phi} \in \mathbb{C}^2$ to the system (5) near $\boldsymbol{\phi}^{(\epsilon=0)}(\boldsymbol{\theta}) \in \mathbb{C}^2$ for every $\epsilon \in \mathcal{O}(0)$ if and only if there exists a unique solution $\boldsymbol{\theta} \in \mathbb{T}^2$ of the system $\boldsymbol{h}(\boldsymbol{\theta}, \epsilon) = 0$ for every $\epsilon \in \mathcal{O}(0)$.

Proof. Representing the unknown solution with $\phi_j = r_j e^{i\theta_j}$, where $r_j \in \mathbb{R}^+$ and $\theta_j \in \mathbb{T}$, we separate the real and imaginary parts in

the form $g_j := \mathrm{Re}(f_j e^{-i\theta_j})$ and $h_j := \mathrm{Im}(f_j e^{-i\theta_j})$. For convenience, we write the explicit expressions:

$$\begin{cases} g_1 := (1-r_1^2)r_1 - \epsilon\,(r_1\cos(2\theta_1) + r_2\cos(\theta_2-\theta_1))\,, \\ g_2 := (1-r_2^2)r_2 - \epsilon\,(r_2\cos(2\theta_2) + r_1\cos(\theta_1-\theta_2)) \end{cases} \tag{7}$$

and

$$\begin{cases} h_1 := \epsilon\,(r_1\sin(2\theta_1) - r_2\sin(\theta_2-\theta_1) + \gamma_1 r_1)\,, \\ h_2 := \epsilon\,(r_2\sin(2\theta_2) - r_1\sin(\theta_1-\theta_2) + \gamma_2 r_2)\,. \end{cases} \tag{8}$$

It is clear that $\boldsymbol{\phi}$ is a root of $\boldsymbol{f}$ if and only if $(\boldsymbol{r},\boldsymbol{\theta}) \in \mathbb{R}^2\times\mathbb{T}^2$ is a root of $(\boldsymbol{g},\boldsymbol{h}) \in \mathbb{R}^2\times\mathbb{R}^2$. Moreover, $(\boldsymbol{g},\boldsymbol{h})$ is smooth both in $(\boldsymbol{r},\boldsymbol{\theta})$ and ϵ.

For $\epsilon = 0$, we pick the solution with $\boldsymbol{r} = \mathbf{1}$ and $\boldsymbol{\theta} \in \mathbb{T}^2$ arbitrary, as per the explicit expression (6). Since $\boldsymbol{g}$ is smooth in $\boldsymbol{r}$, $\boldsymbol{\theta}$, and ϵ, whereas the Jacobian $\partial_{\boldsymbol{u}}\boldsymbol{g}$ at $\boldsymbol{r} = \mathbf{1}$ and $\epsilon = 0$ is invertible, the Implicit Function Theorem for smooth vector functions applies. From this theorem, we deduce the existence of a unique $\boldsymbol{r} \in \mathbb{R}^2$ near $\mathbf{1} \in \mathbb{R}^2$ for every $\boldsymbol{\theta} \in \mathbb{T}^2$ and $\epsilon \in \mathbb{R}$ sufficiently small, such that Eq. (7) is satisfied, the mapping $(\boldsymbol{\theta},\epsilon) \mapsto \boldsymbol{r}$ is smooth and $\|\boldsymbol{r}-\mathbf{1}\| \le C|\epsilon|$ for an ϵ-independent constant $C > 0$.

Substituting the smooth mapping $(\boldsymbol{\theta},\epsilon) \mapsto \boldsymbol{r}$ into the definition of $\boldsymbol{h}$ in Eq. (8), we obtain the smooth function $\boldsymbol{h}(\boldsymbol{\theta},\epsilon) : \mathbb{T}^2\times\mathbb{R} \to \mathbb{R}^2$, the root of which yields the assertion of the lemma. □

Lemma 2.1 represents the first step of the Lyapunov–Schmidt reduction algorithm, namely, a reduction of the original system (5) to the bifurcation equation for the root of a smooth function $\boldsymbol{h}(\boldsymbol{\theta},\epsilon) : \mathbb{T}^2\times\mathbb{R} \to \mathbb{R}^2$, defined from the system (7) and (8). The following lemma represents the second step of the Lyapunov–Schmidt reduction algorithm, namely, a solution of the bifurcation equation in the same limit of small ϵ.

Lemma 2.2. *Denote $\boldsymbol{H}(\boldsymbol{\theta}) = \lim_{\epsilon\to 0}\epsilon^{-1}\boldsymbol{h}(\boldsymbol{\theta},\epsilon)$ and the corresponding Jacobian matrix $\mathcal{N}(\boldsymbol{\theta}) = \partial_{\boldsymbol{\theta}}\boldsymbol{H}(\boldsymbol{\theta})$. Assume that $\boldsymbol{\theta}^{(\epsilon=0)} \in \mathbb{T}^2$ is a root of $\boldsymbol{H}$ such that $\mathcal{N}(\boldsymbol{\theta}^{(\epsilon=0)})$ is invertible. Then, there exists a unique root $\boldsymbol{\theta} \in \mathbb{T}^2$ of $\boldsymbol{h}(\boldsymbol{\theta},\epsilon)$ near $\boldsymbol{\theta}^{(\epsilon=0)}$ for every $\epsilon \in \mathcal{O}(0)$ such that the mapping $\epsilon \mapsto \boldsymbol{\theta}$ is smooth and $\|\boldsymbol{\theta}-\boldsymbol{\theta}^{(\epsilon=0)}\| \le C|\epsilon|$ for an ϵ-independent positive constant C.*

Proof. The particular form in the definition of $\boldsymbol{H}$ relies on the explicit definition (8). The assertion of the lemma follows from the Implicit Function Theorem for smooth vector functions. □

Corollary 2.3. *Under conditions of Lemmas 2.1 and 2.2, there exists a unique solution $\boldsymbol{\phi} \in \mathbb{C}^2$ to the system (5) near $\boldsymbol{\phi}^{(\epsilon=0)}(\boldsymbol{\theta}^{(\epsilon=0)}) \in \mathbb{C}^2$ for every $\epsilon \in \mathcal{O}(0)$ such that the mapping $\epsilon \mapsto \boldsymbol{\phi}$ is smooth and $\|\boldsymbol{\phi}-\boldsymbol{\phi}^{(\epsilon=0)}(\boldsymbol{\theta}^{(\epsilon=0)})\| \le C|\epsilon|$ for an ϵ-independent positive constant C.*

Proof. The proof is just an application of the two-step Lyapunov–Schmidt reduction method. □

In order to classify all possible solutions of the algebraic system (5) for small ϵ, according to the combined result of Lemmas 2.1 and 2.2, we write $\boldsymbol{H}(\boldsymbol{\theta})$ and $\mathcal{N}(\boldsymbol{\theta})$ explicitly as:

$$\boldsymbol{H}(\boldsymbol{\theta}) = \begin{bmatrix} \sin(2\theta_1) - \sin(\theta_2-\theta_1) + \gamma_1 \\ \sin(2\theta_2) - \sin(\theta_1-\theta_2) + \gamma_2 \end{bmatrix} \tag{9}$$

and

$$\mathcal{N}(\boldsymbol{\theta}) = \begin{bmatrix} 2\cos(2\theta_1) + \cos(\theta_2-\theta_1) & -\cos(\theta_2-\theta_1) \\ -\cos(\theta_1-\theta_2) & \cos(\theta_1-\theta_2) + 2\cos(2\theta_2) \end{bmatrix}. \tag{10}$$

Let us simplify the computations in the particular case $\gamma_1 = -\gamma_2 = \gamma$, which corresponds to the symmetric configuration:

(S1S) Symmetry about the vertical and the horizontal lines: $\gamma_1 = -\gamma_2 = \gamma_3 = -\gamma_4$.

In this case, the system $\boldsymbol{H}(\boldsymbol{\theta}) = \mathbf{0}$ is equivalent to the system

$$\begin{cases} \sin(2\theta_1) + \sin(2\theta_2) = 0, \\ \sin(2\theta_1) - \sin(\theta_2-\theta_1) + \gamma = 0. \end{cases} \tag{11}$$

The following list represents all families of solutions of the system (11), which are uniquely continued to the solution of the system (5) for $\epsilon \neq 0$, according to the result of Corollary 2.3.

(1–1) Solving the first equation of system (11) with $2\theta_2 = 2\theta_1 + \pi$ and the second equation with $\sin(2\theta_1) = 1-\gamma$, we obtain a solution for $\gamma \in (0,2)$. Two branches exist for $\theta_1 = \frac{1}{2}\arcsin(1-\gamma)$ and $\theta_1 = \frac{\pi}{2} - \frac{1}{2}\arcsin(1-\gamma)$, which are denoted by (1-1-a) and (1-1-b), respectively. However, the branch (1-1-b) is obtained from the branch (1-1-a) by using symmetries in Remarks 2.1 and 2.3 as well as by flipping the configuration on the left panel of Fig. 1 about the horizontal axis. Therefore, it is sufficient to consider the branch (1-1-a) only. The branch (1-1-a) can be followed in ϵ numerically until at least $\epsilon = 0.3$, where the Jacobian matrix for Eqs. (7) (8) gradually starts becoming more singular.

The Jacobian matrix in (10) is given by

$$2\cos(2\theta_1)\begin{bmatrix} 1 & 0 \\ 0 & -1 \end{bmatrix} \tag{12}$$

and it is invertible if $\cos(2\theta_1) \neq 0$, that is, if $\gamma \neq 0, 2$. In the limit $\gamma \to 0$, the solution $(\phi_1,\phi_2,\phi_3,\phi_4)$ along the branches (1-1-a) and (1-1-b) transforms to the limiting solution $\left(e^{\frac{i\pi}{4}}, e^{\frac{3\pi i}{4}}, e^{\frac{5\pi i}{4}}, e^{\frac{7\pi i}{4}}\right)$, which is the discrete vortex of charge one, according to the terminology in [21]. No vortex of the negative charge one exists for $\gamma \in (0,2)$.

(1–2) Solving the first equation of system (11) with $2\theta_2 = 2\theta_1 - \pi$ and the second equation with $\sin(2\theta_1) = -1-\gamma$, we obtain a solution for $\gamma \in (-2,0)$. Two branches exist for $\theta_1 = -\frac{1}{2}\arcsin(1+\gamma)$ and $\theta_1 = -\frac{\pi}{2} + \frac{1}{2}\arcsin(1+\gamma)$, which are denoted by (1-2-a) and (1-2-b), respectively. Since the branches (1-1-a) and (1-1-b) are connected to the branches (1-2-a) and (1-2-b) by Remark 2.1, it is again sufficient to limit our consideration by branch (1-1-a) for $\gamma \in (0,2)$. In the limit $\gamma \to 0$, the solution $(\phi_1,\phi_2,\phi_3,\phi_4)$ along the branches (1-2-a) and (1-2-b) transforms to the limiting solution $\left(e^{-\frac{i\pi}{4}}, e^{-\frac{3\pi i}{4}}, e^{-\frac{5\pi i}{4}}, e^{-\frac{7\pi i}{4}}\right)$ which is the discrete vortex of the negative charge one. No vortex of the positive charge one exists for $\gamma \in (-2,0)$.

(1–3) Solving the first equation of system (11) with $2\theta_2 = -2\theta_1$ and the second equation with $\sin(2\theta_1) = -\frac{\gamma}{2}$, we obtain a solution for $\gamma \in (-2,2)$. Two branches exist for $\theta_1 = -\frac{1}{2}\arcsin\left(\frac{\gamma}{2}\right)$ and $\theta_1 = \frac{\pi}{2} + \frac{1}{2}\arcsin\left(\frac{\gamma}{2}\right)$, which are denoted by (1-3-a) and (1-3-b), respectively. It is worth mentioning that the expressions for θ_1 as well as

$$r_1 = r_2 = \sqrt{1 - 2\epsilon\cos(2\theta_1)}$$

are exact even if ϵ is not near zero. Due to the existence of the closed-form expressions, both branches in (1-3) will naturally persist in ϵ as long as the expressions hold.

The Jacobian matrix in (10) is given by

$$\cos(2\theta_1)\begin{bmatrix} 3 & -1 \\ -1 & 3 \end{bmatrix}, \tag{13}$$

which is invertible if $\cos(2\theta_1) \neq 0$, that is, if $\gamma \neq \pm 2$. In the limit $\gamma \to 0$, the solution $(\phi_1,\phi_2,\phi_3,\phi_4)$ along the branches (1-3-a) and (1-3-b) transforms to the limiting solutions $(1,1,1,1)$ and $i(1,-1,1,-1)$, which correspond to discrete solitons, according to the terminology in [21].

(1–4) Solving the first equation of system (11) with $2\theta_2 = -2\theta_1 \pm 2\pi$, we obtain the constraint $\gamma = 0$ from the second equation. Therefore, no solutions exist in this choice if $\gamma \neq 0$.

2.2. Symmetry about the center (S2)

Under conditions $\gamma_1 = -\gamma_3$, $\gamma_2 = -\gamma_4$, $\phi_1 = \bar{\phi}_3$, and $\phi_2 = \bar{\phi}_4$, the system (4) reduces to two algebraic equations:

$$\begin{cases} f_1 := (1 - |\phi_1|^2)\phi_1 - \epsilon(\bar{\phi}_2 + \phi_2 - i\gamma_1\phi_1) = 0, \\ f_2 := (1 - |\phi_2|^2)\phi_2 - \epsilon(\bar{\phi}_1 + \phi_1 - i\gamma_2\phi_2) = 0. \end{cases} \tag{14}$$

The system (14) is only slightly different from the system (5). Therefore, Lemmas 2.1 and 2.2 hold for the system (14) and the question of persistence of vortex configurations symmetric about the center can be solved with the two-step Lyapunov–Schmidt reduction algorithm. For explicit computations of the persistence analysis, we obtain the explicit expressions for $\boldsymbol{H}(\boldsymbol{\theta})$ and $\mathcal{N}(\boldsymbol{\theta})$ in Lemma 2.2:

$$\boldsymbol{H}(\boldsymbol{\theta}) = \begin{bmatrix} \sin(\theta_2 + \theta_1) - \sin(\theta_2 - \theta_1) + \gamma_1 \\ \sin(\theta_1 + \theta_2) - \sin(\theta_1 - \theta_2) + \gamma_2 \end{bmatrix} \tag{15}$$

and

$$\mathcal{N}(\boldsymbol{\theta}) = \begin{bmatrix} \cos(\theta_2 + \theta_1) + \cos(\theta_2 - \theta_1) & \cos(\theta_2 + \theta_1) - \cos(\theta_2 - \theta_1) \\ \cos(\theta_1 + \theta_2) - \cos(\theta_1 - \theta_2) & \cos(\theta_1 + \theta_2) + \cos(\theta_1 - \theta_2) \end{bmatrix}. \tag{16}$$

Let us now consider the $\mathcal{PT}$-symmetric network with $\gamma_1 = -\gamma_2 = \gamma$, which corresponds to the symmetric configuration:

(S2S) Symmetry about the horizontal line and the center: $\gamma_1 = -\gamma_2 = -\gamma_3 = \gamma_4$.

Therefore, we rewrite the system $\boldsymbol{H}(\boldsymbol{\theta}) = \boldsymbol{0}$ in the equivalent form:

$$\begin{cases} \sin(\theta_1 + \theta_2) = 0, \\ \sin(\theta_1 - \theta_2) + \gamma = 0. \end{cases} \tag{17}$$

Note in passing that the system (14) admits the exact solution in the polar form $\phi_j = r_j e^{i\theta_j}$, $j = 1, 2$ with

$$r_1 = r_2 = \sqrt{1 - \epsilon\,(\cos(\theta_1 + \theta_2) + \cos(\theta_1 - \theta_2))},$$

where θ_1 and θ_2 are given by the roots of the system (17). The Lyapunov–Schmidt reduction algorithm in Lemmas 2.1 and 2.2 guarantees that these exact solutions are unique in the neighborhood of the limiting solution (6).

The following list represents all families of solutions of the system (17), which are uniquely continued to the solution of the system (14) for $\epsilon \neq 0$, according to the result of Corollary 2.3. Thanks to the explicit expressions for the solutions, the continuation of the solutions occurs even when ϵ is not near zero.

(2–1) $\theta_2 = -\theta_1$ and $\sin(2\theta_1) = -\gamma$ with two branches $\theta_1 = -\frac{1}{2}\arcsin(\gamma)$ and $\theta_1 = \frac{\pi}{2} + \frac{1}{2}\arcsin(\gamma)$ labeled as (2-1-a) and (2-1-b). The two branches exist for $\gamma \in (-1, 1)$. The Jacobian matrix in (16) is given by

$$2\begin{bmatrix} \cos^2(\theta_1) & \sin^2(\theta_1) \\ \sin^2(\theta_1) & \cos^2(\theta_1) \end{bmatrix} \tag{18}$$

and it is invertible if $\cos(2\theta_1) \neq 0$, that is, if $\gamma \neq \pm 1$. In the limit $\gamma \to 0$, the solution $(\phi_1, \phi_2, \phi_3, \phi_4)$ along the branches (2-1-a) and (2-1-b) transforms to the limiting solutions $(1, 1, 1, 1)$ and $i(1, -1, -1, 1)$, which correspond to discrete solitons.

(2–2) $\theta_2 = -\theta_1 \pm \pi$ and $\sin(2\theta_1) = \gamma$ with two branches $\theta_1 = \frac{1}{2}\arcsin(\gamma)$ and $\theta_1 = \frac{\pi}{2} - \frac{1}{2}\arcsin(\gamma)$ labeled as (2-2-a) and (2-2-b). These two branches also exist for $\gamma \in (-1, 1)$. The Jacobian matrix in (16) is given by

$$-2\begin{bmatrix} \cos^2(\theta_1) & \sin^2(\theta_1) \\ \sin^2(\theta_1) & \cos^2(\theta_1) \end{bmatrix}, \tag{19}$$

which is invertible if $\cos(2\theta_1) \neq 0$, that is, if $\gamma \neq \pm 1$. In the limit $\gamma \to 0$, the solution $(\phi_1, \phi_2, \phi_3, \phi_4)$ along the branches (2-2-a) and (2-2-b) transforms to the limiting solutions $(1, -1, 1, -1)$ and $i(1, 1, -1, -1)$, which again correspond to discrete solitons. The family (2-2) is related to the family (2-1) by Remark 2.2.

2.3. Summary on existence results in the elementary cell

We explored two types of gain–loss $\mathcal{PT}$-symmetric configurations in the elementary cell and identified different branches of solutions uniquely continued from $\epsilon = 0$ at a fixed $\gamma \neq 0$.

We conclude that

- the $\mathcal{PT}$-symmetry (S1S) supports vortex configurations (1-1) and (1-2) as well as soliton configurations (1-3).
- the $\mathcal{PT}$-symmetry (S2S) supports only soliton configurations (2-1) and (2-2). Although there exist vortex configurations when $\gamma = 0$, they do not persist with respect to ϵ if $\gamma \neq 0$.

The branch (1-1-a) can be traced numerically with respect to parameter $\epsilon > 0$. The other branches (1-1-b), (1-2-a) and (1-2-b) can be obtained by symmetries given by Remarks 2.1 and 2.3. Also the branches can be extended to $\epsilon < 0$ by using Remark 2.2. The branches (1-3), (2-1) and (2-2) are represented by the exact solutions for $\epsilon \neq 0$.

3. Existence of $\mathcal{PT}$-symmetric vortices in truncated lattice

We shall now consider the $\mathcal{PT}$-symmetric dNLS equation (3) on the square lattice truncated symmetrically with suitable boundary conditions.

For the steady-state solutions $u_{j,k}(\tau) = \phi_{j,k}e^{-4i\epsilon\tau}$, we obtain the stationary $\mathcal{PT}$-symmetric dNLS equation in the form

$$(1 - |\phi_{j,k}|^2)\phi_{j,k} - \epsilon(\phi_{j+1,k} + \phi_{j-1,k} + \phi_{j,k+1} + \phi_{j,k-1} - i\gamma_{j,k}\phi_{j,k}) = 0, \quad (j, k) \in \mathbb{Z}^2. \tag{20}$$

In the limit of $\epsilon \to 0$, we are still looking for the limiting configurations supported on four sites of the elementary cell:

$$\phi_{j,k}^{(\epsilon=0)}(\theta_{j,k}) = e^{i\theta_{j,k}}, \quad (j, k) \in S := \{(1, 0); (1, 1); (0, 1); (0, 0)\}, \tag{21}$$

where $\theta_{j,k} \in \mathbb{T}$ for $(j, k) \in S$, whereas $\phi_{j,k}^{(\epsilon=0)} = 0$ for $(j, k) \in S^* := \mathbb{Z}^2 \backslash S$.

Computations in Section 2 remain valid on the unbounded square lattice, because the results of Lemmas 2.1 and 2.2 are obtained on the set S in the first order in ϵ, where no contributions come from the empty sites in the set S^*.

If the square lattice is truncated, then the truncated square lattice must satisfy the following requirements for persistence of the $\mathcal{PT}$-symmetric configurations:

- the elementary cell S must be central in the symmetric extension of the lattice;
- the distribution of gains and losses in $\{\gamma_{j,k}\}$ must be anti-symmetric with respect to the selected symmetry in Fig. 1, the extended lattice is shown in Fig. 2;
- the boundary conditions must be consistent with the $\mathcal{PT}$-symmetry constraints on $\{\phi_{j,k}\}$.

The periodic boundary conditions may not be consistent with the $\mathcal{PT}$-symmetry constraints because of the jump in the complex phases. On the other hand, Dirichlet conditions at the fixed ends are consistent with the $\mathcal{PT}$-symmetry constraints.

In the following we show continuations of the $\mathcal{PT}$-symmetric solutions from the branches obtained on the elementary cell S in

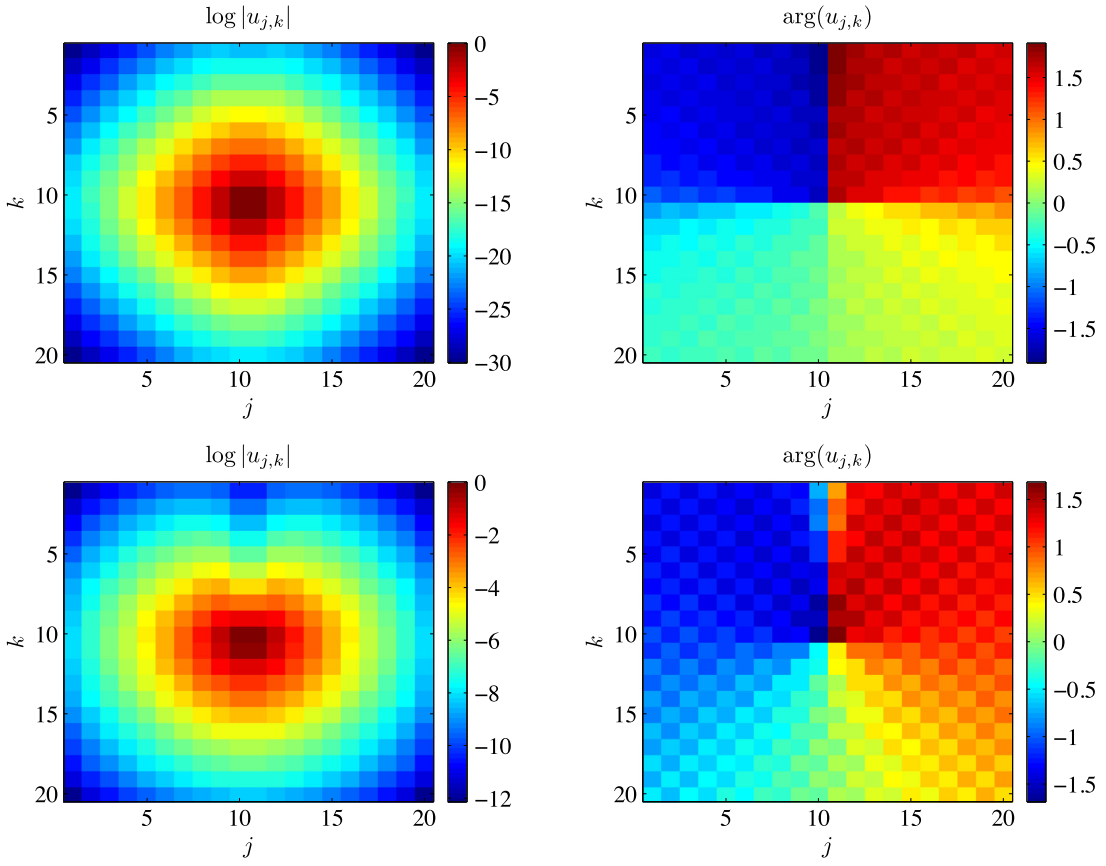

Fig. 3. The top (bottom) row shows the result of continuation of the branch (1-1-a) on the 20-by-20 square lattice to $\gamma_1 = -\gamma_2 = 0.7$ and $\epsilon = 0.1$ ($\epsilon = 0.22$). The left panels show the logarithm of the solution's modulus, and the right panels show the corresponding phase.

Section 2. The relevant configurations are now computed on the 20-by-20 square lattice truncated symmetrically with zero boundary conditions and gain–loss distribution $\gamma_{j,k} = \gamma(-1)^{j+k}$ or $\gamma_{j,k} = \gamma(-1)^k$ that correspond to the bottom panels of Fig. 2. The requirements listed above are satisfied for the truncated square lattice.

(1-1-a) The continuation of the solutions in branch (1-1-a) at $\gamma = 0.7$ is presented in Fig. 3 where the lattice configuration satisfies $\gamma_{j,k} = \gamma(-1)^{j+k}$. The left panels of Fig. 3 illustrate the logarithm of the modulus, while the right panels show the corresponding phase.

At $\epsilon = 0$, the phases of the solution on S in (1-1-a) are $\{\theta_1, \theta_1 + \frac{\pi}{2}, -\theta_1 - \frac{\pi}{2}, -\theta_1\}$, where $\theta_1 = \frac{1}{2}\arcsin(1-\gamma)$. Therefore, the configuration represents the continuation over γ of the discrete vortex of charge one, which corresponds to $\theta_1 = \pi/4$ at $\gamma = 0$. When $\epsilon = 0.1$ is small, we can observe in the top row of Fig. 3 that the solutions are still close to the limiting solutions of $\epsilon = 0$ and the amplitudes are large chiefly at the four central sites of the set S. However, amplitudes of the sites in the set S^* are nonzero for $\epsilon = 0.1$ but still small (at most $\mathcal{O}(\epsilon)$ on the sites of S^* adjacent to the sites of S). At the same time, the phases of the amplitudes on the sites of S do not change much in parameter ϵ and still feature a 2π-change over a discrete contour surrounding the vortex location.

In the bottom panels of Fig. 3, ϵ is set to be 0.22 and the amplitudes are more evenly spread on the lattice although they are still much greater on the sites closer to the center cell. Interestingly, the inequality between the top two sites and the bottom two sites in the center cell at a small ϵ gradually leads to a "heart-shaped" distribution of the amplitudes on the whole lattice.

We notice that the continuations of the solutions in branch (1-1-a) as well as other branches mentioned in Section 2 in finite truncated square lattices can be followed numerically only until some $\epsilon > 0$ (depending on γ and lattice size n), beyond which we can only find a different type of solutions.

(1-3) We present the continuations of the solutions in branches (1-3-a) and (1-3-b) in Figs. 4 and 5, respectively. Again these examples are produced with gain–loss configuration $\gamma_{j,k} = \gamma(-1)^{j+k}$ where $\gamma = 0.7$.

At $\epsilon = 0$, the phases of the solutions on S in (1-3-a) and (1-3-b) are $\{\theta_1, -\theta_1, \theta_1, -\theta_1\}$, where $\theta_1 = -\frac{1}{2}\arcsin(\frac{\gamma}{2})$ or $\theta_1 = \frac{\pi}{2} + \frac{1}{2}\arcsin(\frac{\gamma}{2})$, which represent the continuations over γ of the discrete solitons with $\theta_1 = 0$ or $\pi/2$ at $\gamma = 0$. This interpretation is confirmed by the surface plot for the argument of complex amplitudes in the top panels of Figs. 4 and 5 where $\epsilon = 0.1$ is still close to 0.

As ϵ increases, we are able to track the branches (1-3-a) and (1-3-b) numerically until $\epsilon \approx 0.25$, the examples of which are shown in the bottom panels of Figs. 4 and 5. Unlike the branch (1-1-a), the amplitudes of the solutions in (1-3) spread evenly in both vertical and horizontal directions as ϵ grows.

(2-1) In Figs. 6 and 7, we show the solutions on the square lattice that are continued from the branches (2-1-a) and (2-1-b) in Section 2. In these examples we set $\gamma_{j,k} = \gamma(-1)^k$ and $\gamma = 0.8$.

At $\epsilon = 0$, the solutions on S in (2-1-a) and (2-1-b) have phases $\{\theta_1, -\theta_1, -\theta_1, \theta_1\}$, where $\theta_1 = \frac{1}{2}\arcsin(\frac{\gamma}{2})$ or $\theta_1 = \frac{\pi}{2} - \frac{1}{2}\arcsin(\frac{\gamma}{2})$. These configurations represent the continuations over γ of the discrete solitons with $\theta_1 = 0$

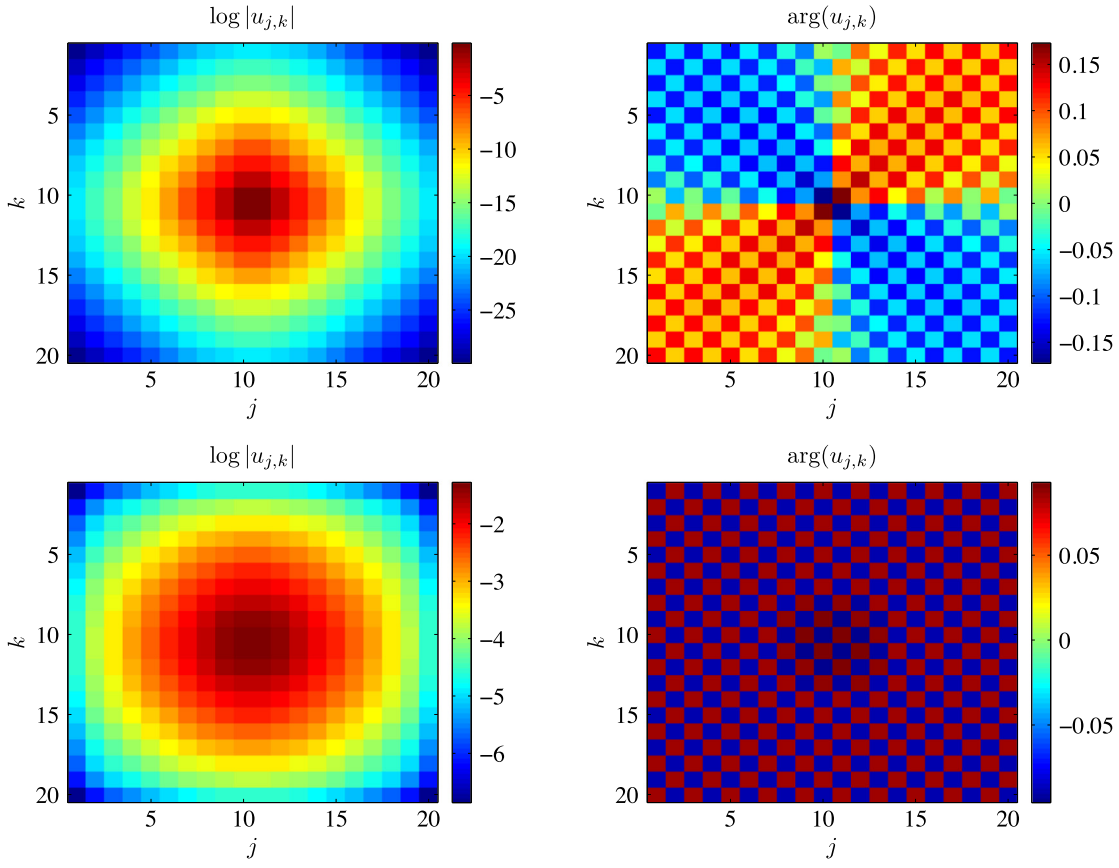

Fig. 4. The top (bottom) row shows the result of continuation of the branch (1-3-a) on the 20-by-20 square lattice to $\gamma_1 = -\gamma_2 = 0.7$ and $\epsilon = 0.1$ ($\epsilon = 0.25$). The left panels show the logarithm of the solution's modulus, and the right panels show the corresponding phase.

or $\pi/2$ at $\gamma = 0$. In the top panels of Figs. 6 and 7, it can be seen that the phases of the amplitudes on the sites of S still feature a clearly discernible discrete soliton.

In the bottom panels of Figs. 6 and 7, we follow the continuations of branches (2-1-a) and (2-1-b) in the lattice until $\epsilon = 0.25$ and $\epsilon = 0.22$, respectively. Here we notice the transferring of the amplitudes from the center sites to the whole lattice favors the vertical direction in both configurations, although it is much easier to be observed in the bottom left panel of Fig. 7.

(2-2) Again $\gamma_{j,k} = \gamma(-1)^k$ and $\gamma = 0.8$, we show the continuations of the solutions from branches (2-2-a) and (2-2-b) in the square lattice in Figs. 8 and 9.

At $\epsilon = 0$, the phases of the solutions on S in (2-2-a) and (2-2-b) are $\{\theta_1, \pi - \theta_1, -\theta_1, \theta_1 - \pi\}$, where $\theta_1 = \frac{1}{2}\arcsin(\gamma)$ or $\theta_1 = \frac{\pi}{2} - \frac{1}{2}\arcsin(\gamma)$. At $\gamma = 0$ these configurations correspond to the discrete solitons with $\theta_1 = 0$ or $\pi/2$. The case when $\epsilon = 0.1$ is shown by the surface plot for the argument of complex amplitudes in the top panels of Figs. 8 and 9.

In the bottom panels of Figs. 8 and 9, we show the continuations of branches (2-2-a) and (2-2-b) in the lattice at $\epsilon = 0.25$ and $\epsilon = 0.22$, respectively. From both figures, we clearly see that the whole lattice features a "dumbbell" shape.

To summarize, we have set the elementary cell in Section 2 to be the central cell of a square lattice and examined the continuations of the single-cell solutions in the truncated lattice. We have generically found that the main results in Section 2 represent branches of solutions in the truncated lattice.

We mainly studied two types of gain–loss structures of the lattice, namely $\gamma_{j,k} = \gamma(-1)^{j+k}$ and $\gamma_{j,k} = \gamma(-1)^k$. We also monitored the continuation of the solutions from each branch in ϵ numerically and found that these solutions can be followed up to some ϵ that may depend on γ and the lattice size.

4. Stability of $\mathcal{PT}$-symmetric configurations in the cell

We address the $\mathcal{PT}$-symmetric configurations in the elementary cell consisting of four sites. Persistence of these configurations in the small parameter ϵ is obtained in Section 2. In what follows, we consider spectral stability of the $\mathcal{PT}$-symmetric configurations.

Let $\boldsymbol{\phi} := \{\phi_j\}_{1\le j\le 4}$ be a stationary solution of the system (4). If it is $\mathcal{PT}$-symmetric, there exists a 4-by-4 matrix P such that $\bar{\boldsymbol{\phi}} = P\boldsymbol{\phi}$. For the two $\mathcal{PT}$-symmetries considered in Section 2, we list the matrix P:

$$\text{(S1)}\quad P = \begin{pmatrix} 0 & 0 & 0 & 1 \\ 0 & 0 & 1 & 0 \\ 0 & 1 & 0 & 0 \\ 1 & 0 & 0 & 0 \end{pmatrix}, \qquad \text{(S2)}\quad P = \begin{pmatrix} 0 & 0 & 1 & 0 \\ 0 & 0 & 0 & 1 \\ 1 & 0 & 0 & 0 \\ 0 & 1 & 0 & 0 \end{pmatrix}. \tag{22}$$

Adding a perturbation to the steady-state solution, we write

$$u_j(\tau) = \left(\phi_j + \delta\left[e^{\lambda\tau} v_j + e^{\bar{\lambda}\tau}\overline{w_j}\right]\right) e^{-2i\epsilon\tau},$$

where δ is the perturbation amplitude, $\lambda \in \mathbb{C}$ is the spectral parameter, and $(\boldsymbol{v}, \boldsymbol{w}) := \{(v_j, w_j)\}_{1\le j\le 4}$ represents an eigenvector

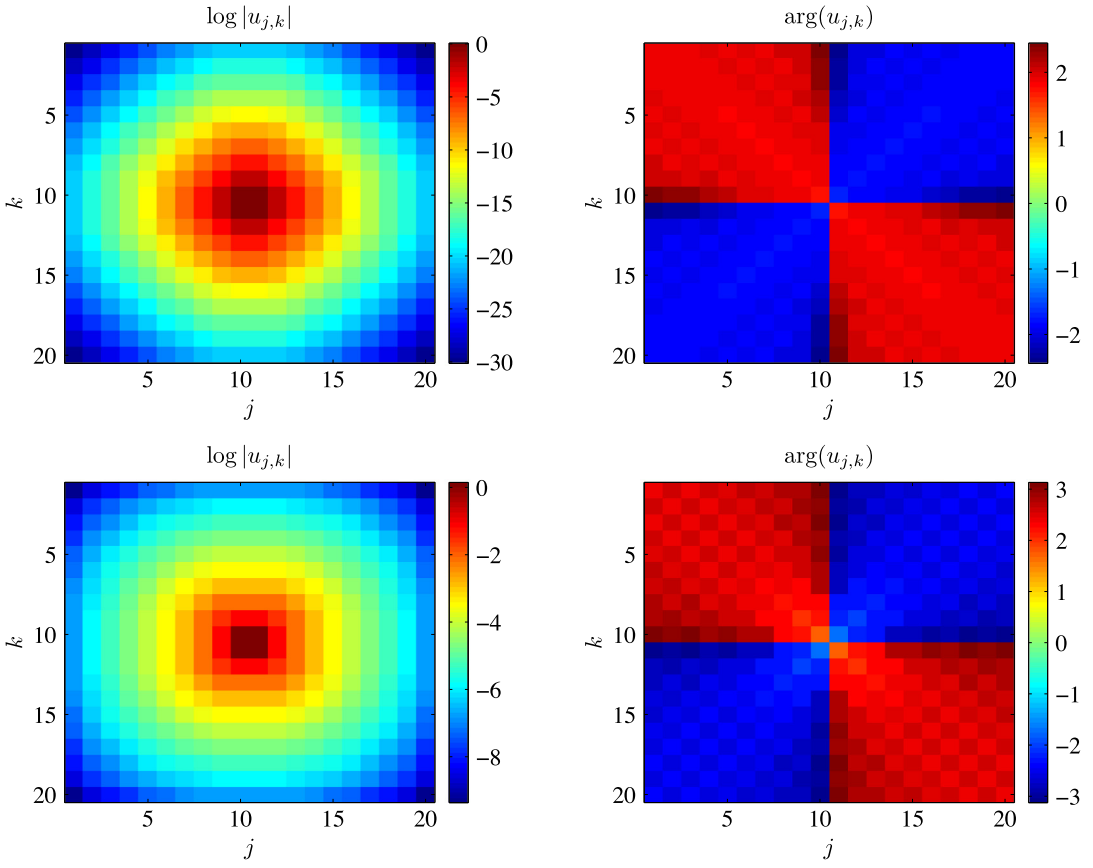

Fig. 5. The top (bottom) row shows the result of continuation of the branch (1-3-b) on the 20-by-20 square lattice to $\gamma_1 = -\gamma_2 = 0.7$ and $\epsilon = 0.1$ ($\epsilon = 0.24$). The left panels show the logarithm of the solution's modulus, and the right panels show the corresponding phase.

of the spectral stability problem. After the linearization of the $\mathcal{PT}$-symmetric dNLS equation (3) at the four-site cell, we obtain the spectral stability problem in the form

$$\begin{cases} i\lambda v_j = (1 + i\epsilon\gamma_j - 2|\phi_j|^2)v_j - (\phi_j)^2 w_j - \epsilon(v_{j-1} + v_{j+1}), \\ -i\lambda w_j = -(\overline{\phi}_j)^2 v_j + (1 - i\epsilon\gamma_j - 2|\phi_j|^2)w_j - \epsilon(w_{j-1} + w_{j+1}), \end{cases} \quad 1 \le j \le 4, \tag{23}$$

where cyclic boundary conditions on $\{(v_j, w_j)\}_{1\le j\le 4}$ are assumed.

The eigenvalue problem (23) can be written in the matrix form

$$i\lambda\sigma\boldsymbol{\xi} = (\mathcal{H} + i\epsilon\mathcal{G})\,\boldsymbol{\xi}, \tag{24}$$

where $\boldsymbol{\xi}$ consists of blocks of $(v_j, w_j)^T$, σ consists of blocks of Pauli matrices $\sigma_3 = \mathrm{diag}(1, -1)$, $\mathcal{G}$ consists of blocks of $\gamma_j\sigma_3$, and $\mathcal{H}$ is the Hermitian matrix consisting of the blocks of

$$\mathcal{H}_j = \begin{pmatrix} 1 - 2|\phi_j|^2 & -(\phi_j)^2 \\ -(\overline{\phi}_j)^2 & 1 - 2|\phi_j|^2 \end{pmatrix} - \epsilon(s_{+1} + s_{-1}) \begin{pmatrix} 1 & 0 \\ 0 & 1 \end{pmatrix}, \tag{25}$$

where s_j stands for the shift operator such that $(s_j\phi)_k = \phi_{k+j}$.

Remark 4.1. If λ is an eigenvalue of the spectral problem (23) with the eigenvector $(\boldsymbol{v}, \boldsymbol{w})$, then $\bar{\lambda}$ is another eigenvalue of the same problem (23) with the eigenvector $(\bar{\boldsymbol{w}}, \bar{\boldsymbol{v}})$. Therefore, eigenvalues λ are symmetric about the real axis.

Remark 4.2. Assume that $\boldsymbol{\phi}$ is $\mathcal{PT}$-symmetric, so that $\bar{\boldsymbol{\phi}} = P\boldsymbol{\phi}$ for P given by (22). If λ is an eigenvalue of the spectral problem (23) with the eigenvector $(\boldsymbol{v}, \boldsymbol{w})$, then $-\bar{\lambda}$ is another eigenvalue of the same problem (23) with the eigenvector $(P\bar{\boldsymbol{v}}, P\bar{\boldsymbol{w}})$. Therefore, eigenvalues λ are symmetric about the imaginary axis.

In order to study stability of the stationary solutions in the limit of small ϵ, we adopt the stability results obtained in [21]. Along this way, it is easier to work with a stationary solution $\boldsymbol{\phi}$ without using the property of $\mathcal{PT}$-symmetry. Nevertheless, it is true that ϕ_3 and ϕ_4 are expressed from ϕ_1 and ϕ_2 by using the matrix P given by (22). With the account of the relevant symmetry, Corollary 2.3 implies that the stationary solution can be expressed in the form

$$\phi_j = e^{i\theta_j^{(0)}} \left[1 + \epsilon r_j^{(1)} + i\epsilon\left(\theta_j^{(1)} - \theta_j^{(0)}\right) + \mathcal{O}(\epsilon^2)\right], \quad 1 \le j \le 4, \tag{26}$$

where $\{\theta_j^{(0)}\}_{1\le j\le 4}$ are determined from simple roots of the vector function $\boldsymbol{H}$, $\{\theta_j^{(1)}\}_{1\le j\le 4}$ are found from persistence analysis in Lemma 2.2, and $\{r_j^{(1)}\}_{1\le j\le 4}$ are found from persistence analysis in Lemma 2.1. After elementary computations, we obtain the explicit expression

$$r_j^{(1)} = -\frac{1}{2}\left[\cos(\theta_j^{(0)} - \theta_{j-1}^{(0)}) + \cos(\theta_j^{(0)} - \theta_{j+1}^{(0)})\right], \tag{27}$$

where the cyclic boundary conditions for $\{\theta_j^{(0)}\}_{1\le j\le 4}$ are assumed. For convenience of our presentation, we drop the superscripts in writing $\theta_j^{(0)}$.

Let $\mathcal{M}$ be a 4-by-4 matrix satisfying

$$\mathcal{M}_{j,k} = \begin{cases} \cos(\theta_j - \theta_{j-1}) + \cos(\theta_j - \theta_{j+1}), & k = j \\ -\cos(\theta_j - \theta_{j-1}), & k = j-1 \\ -\cos(\theta_j - \theta_{j+1}), & k = j+1 \\ 0, & \text{otherwise.} \end{cases} \tag{28}$$

Due to the gauge invariance of the original dNLS equation (3), $\mathcal{M}$ always has a zero eigenvalue with eigenvector $(1, 1, 1, 1)^T$. The

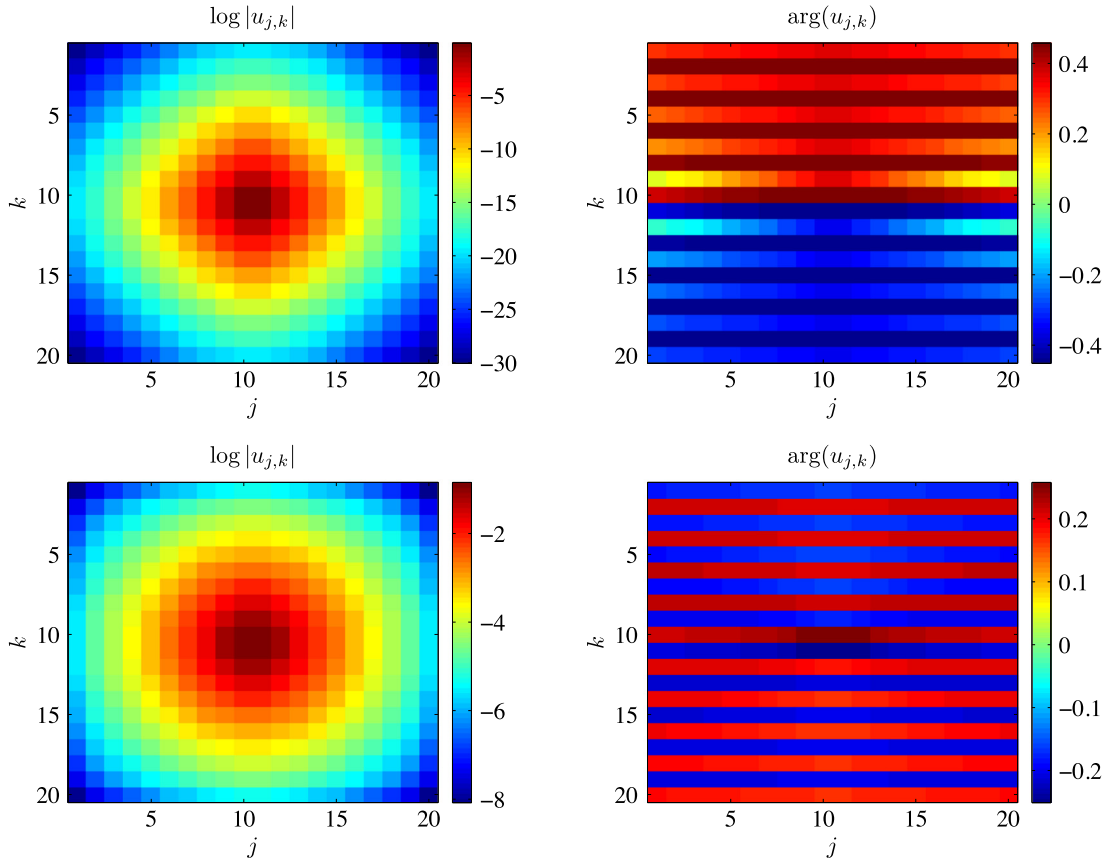

Fig. 6. The top (bottom) row shows the result of continuation of the branch (2-1-a) on the 20-by-20 square lattice to $\gamma_1 = -\gamma_2 = 0.8$ and $\epsilon = 0.1$ ($\epsilon = 0.25$). The left panels show the logarithm of the solution's modulus, and the right panels show the corresponding phase.

other three eigenvalues of $\mathcal{M}$ may be nonzero. As is established in [21], the nonzero eigenvalues of the matrix $\mathcal{M}$ are related to small eigenvalues of the matrix operator $\mathcal{H}$ of the order of $\mathcal{O}(\epsilon)$. In order to render the stability analysis herein self-contained, we review the statement and the proof of this result.

Lemma 4.1. *Let μ_j be a nonzero eigenvalue of the matrix $\mathcal{M}$. Then, for sufficiently small $\epsilon \in \mathcal{O}(0)$, the matrix operator $\mathcal{H}$ has a small nonzero eigenvalue ν_j such that*

$$\nu_j = \mu_j \epsilon + \mathcal{O}(\epsilon^2). \tag{29}$$

Proof. We consider the expansion $\mathcal{H} = \mathcal{H}^{(0)} + \epsilon \mathcal{H}^{(1)} + O(\epsilon^2)$, where $\mathcal{H}^{(0)}$ consists of the blocks

$$\mathcal{H}_j^{(0)} = \begin{pmatrix} -1 & -e^{2i\theta_j} \\ -e^{-2i\theta_j} & -1 \end{pmatrix}. \tag{30}$$

Each block has a one-dimensional kernel spanned by the vector $(e^{i\theta_j}, -e^{-i\theta_j})$. Let $\boldsymbol{e_j}$ be the corresponding eigenvector of $\mathcal{H}^{(0)}$ for the zero eigenvalue. Therefore, we have

$$\ker(\mathcal{H}^{(0)}) = \text{span}\{\boldsymbol{e_j}\}_{1 \le j \le 4}.$$

By regular perturbation theory, we are looking for the small eigenvalue ν_j and eigenvector $\boldsymbol{\eta}$ of the Hermitian matrix operator $\mathcal{H}$ for small $\epsilon \in \mathcal{O}(0)$ in the form

$$\nu_j = \epsilon \nu_j^{(1)} + \mathcal{O}(\epsilon^2), \qquad \boldsymbol{\eta} = \boldsymbol{\eta}^{(0)} + \epsilon \boldsymbol{\eta}^{(1)} + \mathcal{O}(\epsilon^2),$$

where $\boldsymbol{\eta}^{(0)} = \sum_{j=1}^{4} c_j \boldsymbol{e_j}$ and $\{c_j\}_{1 \le j \le 4}$ are to be determined. At the first order of $\mathcal{O}(\epsilon)$, we obtain the linear inhomogeneous system

$$\mathcal{H}^{(0)} \boldsymbol{\eta}^{(1)} + \mathcal{H}^{(1)} \boldsymbol{\eta}^{(0)} = \nu_j^{(1)} \boldsymbol{\eta}^{(0)}, \tag{31}$$

where $\mathcal{H}^{(1)}$ consists of the blocks

$$\mathcal{H}_j^{(1)} = -2r_j^{(1)} \begin{pmatrix} 2 & e^{2i\theta_j} \\ e^{-2i\theta_j} & 2 \end{pmatrix} - (s_{+1} + s_{-1}) \begin{pmatrix} 1 & 0 \\ 0 & 1 \end{pmatrix} \tag{32}$$

where the expansion (26) has been used. Projection of the linear inhomogeneous equation (31) to $\ker(\mathcal{H}^{(0)})$ gives the 4-by-4 matrix eigenvalue problem

$$\mathcal{M} \boldsymbol{c} = \nu_j^{(1)} \boldsymbol{c}, \tag{33}$$

where $\mathcal{M}_{j,k} = \frac{1}{2} \langle \boldsymbol{e_j}, \mathcal{H}^{(1)} \boldsymbol{e_k} \rangle$ is found to coincide with the one given by (28) thanks to the explicit expressions (27). □

We will now prove that the small nonzero eigenvalues of $\mathcal{H}$ for small nonzero ϵ determine the small eigenvalues in the spectral stability problem (24). The following lemma follows the approach of [21] but incorporates the additional term $i\epsilon \mathcal{G}$ due to the $\mathcal{PT}$-symmetric gain and loss terms.

Lemma 4.2. *Let μ_j be a nonzero eigenvalue of the matrix $\mathcal{M}$. Then, for sufficiently small $\epsilon \in \mathcal{O}(0)$, the spectral problem (24) has a pair of small nonzero eigenvalues $\pm\lambda_j$ such that*

$$\lambda_j^2 = 2\mu_j \epsilon + \mathcal{O}(\epsilon^2). \tag{34}$$

Proof. We recall that $\ker(\mathcal{H}^{(0)}) = \text{span}\{\boldsymbol{e_j}\}_{1 \le j \le 4}$. Let $\hat{\boldsymbol{e}}_j = \sigma \boldsymbol{e_j}$. Then, $\mathcal{H}^{(0)} \hat{\boldsymbol{e}}_j = -2\hat{\boldsymbol{e}}_j$. Since the operator $\sigma \mathcal{H}^{(0)}$ is not self-adjoint, the zero eigenvalue of $\mathcal{H}^{(0)}$ of geometric multiplicity 4 may become a defective zero eigenvalue of $\mathcal{H}^{(0)}$ of higher algebraic multiplicity. As is well-known [21], the zero eigenvalue of $\mathcal{H}^{(0)}$ has

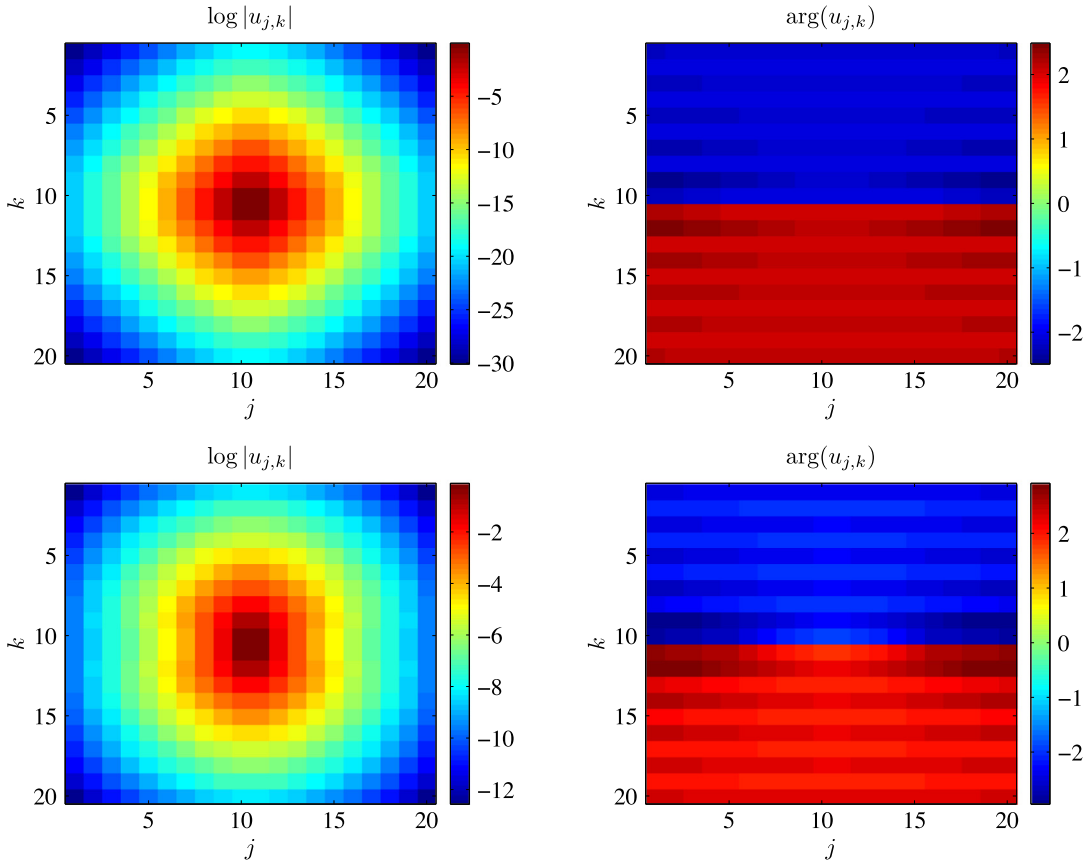

Fig. 7. The top (bottom) row shows the result of continuation of the branch (2-1-b) on the 20-by-20 square lattice to $\gamma_1 = -\gamma_2 = 0.8$ and $\epsilon = 0.1$ ($\epsilon = 0.22$). The left panels show the logarithm of the solution's modulus, and the right panels show the corresponding phase.

algebraic multiplicity 8 with

$$\ker(\sigma\mathcal{H}^{(0)}) = \text{span}\{\boldsymbol{e_j}\}_{1\le j\le 4} \quad \text{and}$$
$$\ker((\sigma\mathcal{H}^{(0)})^2) = \text{span}\{\boldsymbol{e_j}, \hat{\boldsymbol{e}}_{\boldsymbol{j}}\}_{1\le j\le 4}.$$

By the regular perturbation theory for two-dimensional Jordan blocks, we are looking for the small eigenvalue λ_j and eigenvector $\boldsymbol{\xi}$ of the spectral problem (24) for small $\epsilon \in \mathcal{O}(0)$ in the form

$$\lambda_j = \epsilon^{1/2}\lambda_j^{(1)} + \epsilon\lambda_j^{(2)} + \mathcal{O}(\epsilon^{3/2}),$$
$$\boldsymbol{\xi} = \boldsymbol{\xi}^{(0)} + \epsilon^{1/2}\boldsymbol{\xi}^{(1)} + \epsilon\boldsymbol{\xi}^{(2)} + \mathcal{O}(\epsilon^{3/2}),$$

where $\boldsymbol{\xi}^{(0)} = \sum_{j=1}^{4} c_j\boldsymbol{e_j}$ and $\{c_j\}_{1\le j\le 4}$ are to be determined. At the first order of $\mathcal{O}(\epsilon^{1/2})$, we obtain the linear inhomogeneous system

$$\mathcal{H}^{(0)}\boldsymbol{\xi}^{(1)} = i\lambda_j^{(1)}\sigma\boldsymbol{\xi}^{(0)}. \tag{35}$$

Since $\sigma\mathcal{H}^{(0)}\hat{\boldsymbol{e}}_{\boldsymbol{j}} = -2\boldsymbol{e_j}$, we obtain the explicit solution of the linear inhomogeneous equation (35) in the form

$$\boldsymbol{\xi}^{(1)} = -\frac{i\lambda_j^{(1)}}{2}\sum_{j=1}^{4} c_j\hat{\boldsymbol{e}}_{\boldsymbol{j}}.$$

At the second order of $\mathcal{O}(\epsilon)$, we obtain the linear inhomogeneous system

$$\mathcal{H}^{(0)}\boldsymbol{\xi}^{(2)} + \mathcal{H}^{(1)}\boldsymbol{\xi}^{(0)} + i\mathcal{G}\boldsymbol{\xi}^{(0)} = i\lambda_j^{(1)}\sigma\boldsymbol{\xi}^{(1)} + i\lambda_j^{(2)}\sigma\boldsymbol{\xi}^{(0)}. \tag{36}$$

Projection of the linear inhomogeneous equation (36) to $\ker(\mathcal{H}^{(0)})$ gives the 4-by-4 matrix eigenvalue problem

$$\mathcal{M}\boldsymbol{c} = \frac{1}{2}(\lambda_j^{(1)})^2\boldsymbol{c}, \tag{37}$$

since $\langle\boldsymbol{e_j}, \mathcal{G}\boldsymbol{e_k}\rangle = 0$ for every j, k. Thus, the additional term $i\epsilon\mathcal{G}$ due to the $\mathcal{PT}$-symmetric gain and loss terms does not contribute to the leading order of the nonzero eigenvalues λ_j, which split according to the asymptotic expansion (34). Note that the relevant eigenvalues still depend on the gain–loss parameter γ, due to the dependence of the parameters $\{\theta_j\}_{1\le j\le 4}$ on γ. □

If the stationary solution $\{\phi_j\}_{1\le j\le 4}$ satisfies the $\mathcal{PT}$-symmetry, that is, $\bar{\boldsymbol{\phi}} = P\boldsymbol{\phi}$ with P given by (22), then the 4-by-4 matrix $\mathcal{M}$ given by (28) has additional symmetry and can be folded into two 2-by-2 matrices. One of these two matrices must have nonzero eigenvalues because the $\mathcal{PT}$-symmetric configuration $\boldsymbol{\phi}$ persists with respect to the small parameter ϵ by Corollary 2.3. The other matrix must have a zero eigenvalue due to the gauge invariance of the system of stationary equations (4). Since the persistence analysis depends on the $\mathcal{PT}$-symmetry and different solution branches have been identified in each case, we continue separately for the two kinds of the $\mathcal{PT}$-symmetry on the elementary cell studied in Section 2.

4.1. Symmetry about the vertical line (S1)

Under conditions $\gamma_1 = -\gamma_4$ and $\gamma_2 = -\gamma_3$, we consider the $\mathcal{PT}$-symmetric configuration in the form $\phi_1 = \bar{\phi}_4$ and $\phi_2 = \bar{\phi}_3$. Thus, we have $\theta_1 = -\theta_4$ and $\theta_2 = -\theta_3$, after which the 4-by-4 matrix $\mathcal{M}$ given by (28) can be written in the explicit form:

$$\mathcal{M} = \begin{pmatrix} a+b & -b & 0 & -a \\ -b & b+c & -c & 0 \\ 0 & -c & b+c & -b \\ -a & 0 & -b & a+b \end{pmatrix},$$

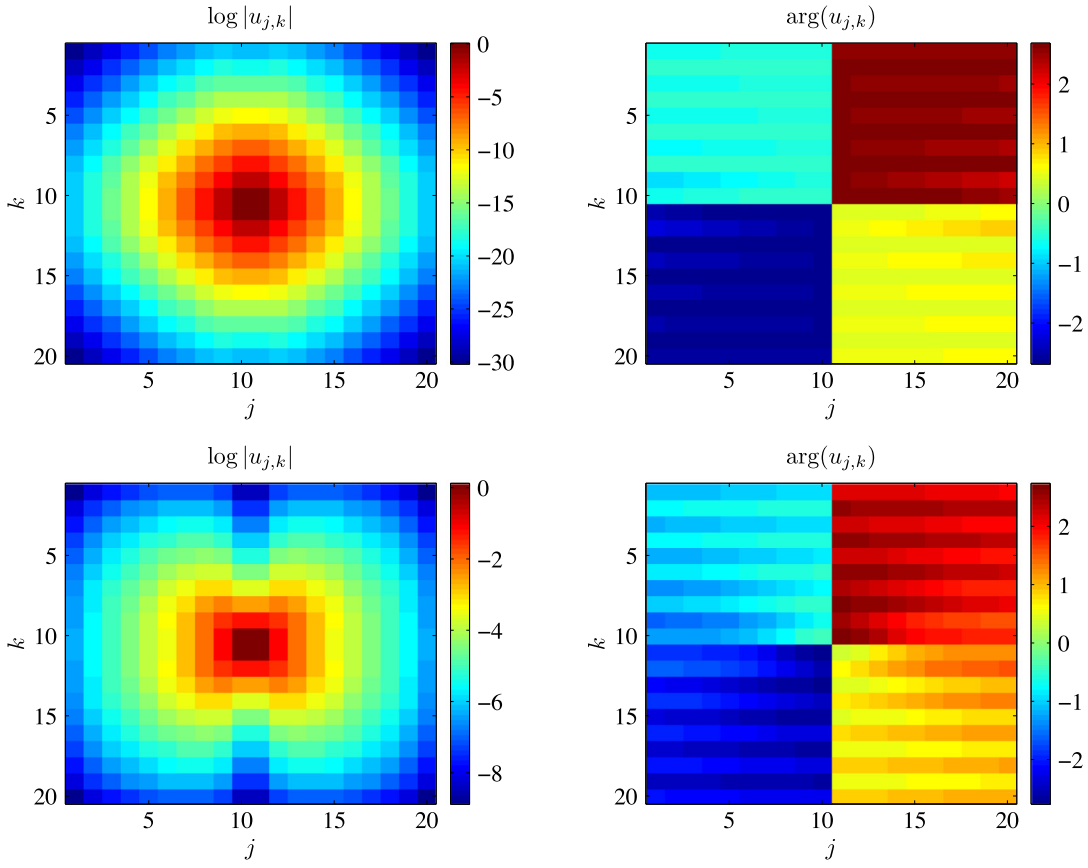

Fig. 8. The top (bottom) row shows the result of continuation of the branch (2-2-a) on the 20-by-20 square lattice to $\gamma_1 = -\gamma_2 = 0.8$ and $\epsilon = 0.1$ ($\epsilon = 0.25$). The left panels show the logarithm of the solution's modulus, and the right panels show the corresponding phase.

where $a = \cos(2\theta_1)$, $b = \cos(\theta_1 - \theta_2)$, and $c = \cos(2\theta_2)$. Using the transformation matrix

$$T = \begin{pmatrix} 1 & 0 & 0 & 1 \\ 0 & 1 & 1 & 0 \\ 0 & 1 & -1 & 0 \\ 1 & 0 & 0 & -1 \end{pmatrix},$$

which generalizes the matrix P given by (22) for (S1), we obtain the block-diagonalized form of the matrix M after a similarity transformation:

$$T^{-1}MT = \begin{pmatrix} b & -b & 0 & 0 \\ -b & b & 0 & 0 \\ 0 & 0 & b+2c & -b \\ 0 & 0 & -b & 2a+b \end{pmatrix}.$$

Note that the first block is given by a singular matrix, whereas the second block coincides with the Jacobian matrix $\mathcal{N}(\boldsymbol{\theta})$ given by (10).

The following list summarizes the stability features of the irreducible branches (1-1-a), (1-3-a), and (1-3-b) among solutions of the system (11), which corresponds to the particular symmetry (S1S) with $\gamma_1 = -\gamma_2 = \gamma$.

(1-1-a) For the solution with $2\theta_2 = 2\theta_1 + \pi$ and $\sin(2\theta_1) = 1 - \gamma$, we obtain $a = -c = \cos(2\theta_1)$ and $b = 0$. Therefore, the matrix $\mathcal{M}$ has a double zero eigenvalue with eigenvectors $(1, 0, 0, 1)^T$, $(0, 1, 1, 0)^T$ and a pair of simple nonzero eigenvalues $\mu_\pm = \pm 2\cos(2\theta_1)$ with eigenvectors $(-1, 0, 0, 1)^T$ and $(0, -1, 1, 0)^T$.

By Lemma 4.2, the spectral stability problem (24) has two pairs of small nonzero eigenvalues λ: one pair of λ is purely real near $\pm\sqrt{|4\epsilon\cos(2\theta_1)|}$ and another pair of λ is purely imaginary near $\pm i\sqrt{|4\epsilon\cos(2\theta_1)|}$ as $\epsilon \to 0$. Therefore, the branch (1-1-a) corresponding to the vortex configurations is spectrally unstable. This instability disappears in the limit of $\gamma \to 0$, as $\theta_1 \to \pi/4$ in this limit, and the dependence of the relevant eigenvalue emerges at a higher order in ϵ, with the eigenvalue being imaginary [21].

Fig. 10 shows comparisons between the eigenvalues approximated using the first-order reductions in Lemma 4.2 and those computed numerically for the branch (1-1-a) with $\epsilon > 0$. Note that one of the pairs of real eigenvalues (second thickest solid blue line) appears beyond the first-order reduction of Lemma 4.2 (see [21] for further details).

(1-3) For the solution with $2\theta_2 = -2\theta_1$ and $\sin(2\theta_1) = -\frac{\gamma}{2}$, we obtain $a = b = c = \cos(2\theta_1)$. Therefore, the matrix $\mathcal{M}$ has a simple zero eigenvalue $\mu_1 = 0$ with eigenvector $(1, 1, 1, 1)^T$, a double nonzero eigenvalue $\mu_2 = \mu_3 = 2\cos(2\theta_1)$ with eigenvectors $(i, -1, -i, 1)^T$ and $(-i, -1, i, 1)^T$, and a simple nonzero eigenvalue $\mu_4 = 4\cos(2\theta_1)$ with eigenvector $(-1, 1, -1, 1)^T$.

Now we can distinguish between the branches (1-3-a) and (1-3-b) which correspond to $\theta_1 = -\frac{1}{2}\arcsin\left(\frac{\gamma}{2}\right)$ and $\theta_1 = \frac{\pi}{2} + \frac{1}{2}\arcsin\left(\frac{\gamma}{2}\right)$ respectively.

By Lemma 4.2, the spectral stability problem (24) for the branch (1-3-a) has only pairs of real eigenvalues λ, moreover, the pair of double real eigenvalues in the first-order reduction may split to a complex quartet beyond the first-order reduction. Independently of the outcome of this splitting, the branch (1-3-a) is spectrally unstable.

On the other hand, the spectral stability problem (24) for the branch (1-3-b) has only pairs of imaginary eigenvalues

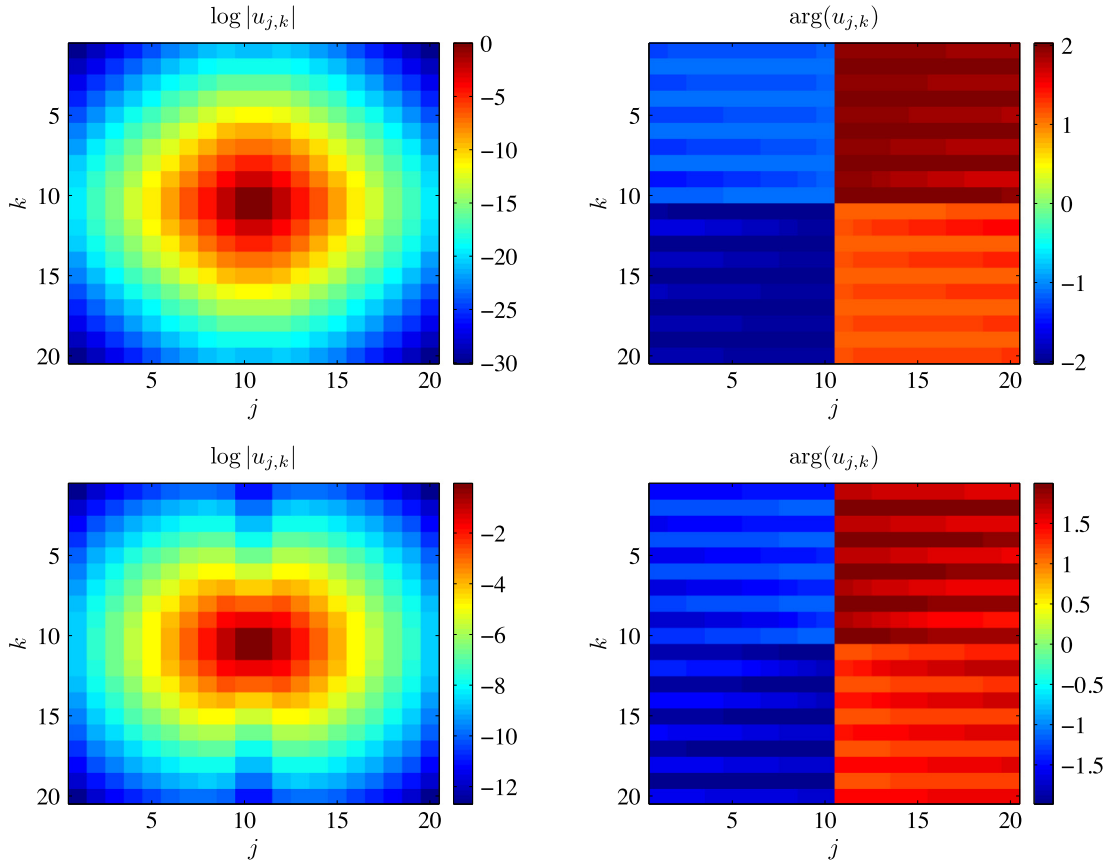

Fig. 9. The top (bottom) row shows the result of continuation of the branch (2-2-b) on the 20-by-20 square lattice to $\gamma_1 = -\gamma_2 = 0.8$ and $\epsilon = 0.1$ ($\epsilon = 0.22$). The left panels show the logarithm of the solution's modulus, and the right panels show the corresponding phase.

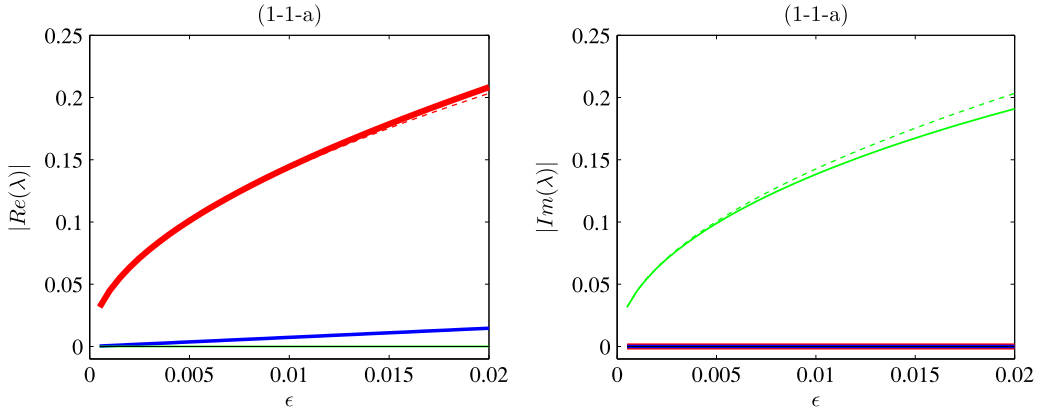

Fig. 10. The real (left) and imaginary (right) parts of eigenvalues λ as functions of ϵ at $\gamma = 1 + \frac{\sqrt{3}}{2}$ for the branch (1-1-a) in comparison with the analytically approximated eigenvalues (dashed lines). In the left panel, two thinner (green and black) lines are zero, the thickest (red) line is predicted by the asymptotic theory, and the thicker (blue) line appears beyond the leading-order asymptotic theory. In the right panel, the thinner (green) line is predicted by the asymptotic theory whereas all other (red, blue and black) lines are identically zero. (For interpretation of the references to color in this figure legend, the reader is referred to the web version of this article.)

λ in the first-order reduction in ϵ. However, one pair of imaginary eigenvalues λ is double and may split to a complex quartet beyond the first-order reduction. If this splitting actually occurs, the branch (1-3-b) is spectrally unstable as well.

Figs. 11 and 12 illustrate the comparisons between numerical eigenvalues and approximated eigenvalues for the branches (1-3-a) and (1-3-b) respectively. We can see that the pair of double real eigenvalues λ of the spectral stability problem (24) for the branch (1-3-a) splits into two pairs of simple real eigenvalues, hence the complex quartets do not appear as a result of this splitting. On the other hand, the pair of double imaginary eigenvalues λ of the spectral stability problem (24) for the branch (1-3-b) does split into a quartet of complex eigenvalues, which results in the (weak) spectral instability of the branch (1-3-b).

4.2. Symmetry about the center (S2)

Under conditions $\gamma_1 = -\gamma_3$ and $\gamma_2 = -\gamma_4$, we consider the $\mathcal{PT}$-symmetric configuration in the form $\phi_1 = \bar{\phi}_3$ and $\phi_2 = \bar{\phi}_4$.

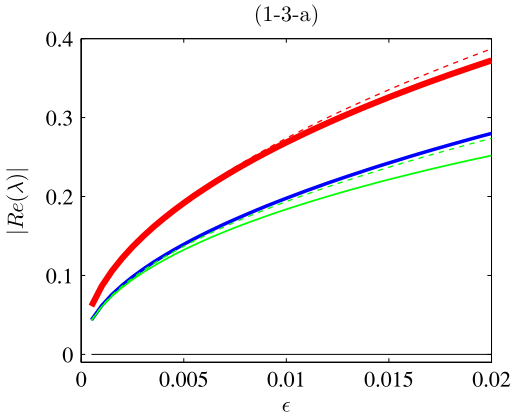

Fig. 11. The real parts of eigenvalues λ as functions of ϵ at $\gamma = -0.7$ for the branch (1-3-a) in comparison with the analytically approximated eigenvalues (dashed lines). The imaginary parts are identically zero. The double real eigenvalue splits beyond the leading-order asymptotic theory. As in Fig. 10, in this figure and the following figures of this section, we use lines of different thicknesses (and different colors if online) to represent different eigenvalues as functions of ϵ.

Thus, we have $\theta_1 = -\theta_3$ and $\theta_2 = -\theta_4$, after which the 4-by-4 matrix $\mathcal{M}$ given by (28) can be written in the explicit form:

$$\mathcal{M} = \begin{pmatrix} a+b & -b & 0 & -a \\ -b & a+b & -a & 0 \\ 0 & -a & a+b & -b \\ -a & 0 & -b & a+b \end{pmatrix},$$

where $a = \cos(\theta_1 + \theta_2)$ and $b = \cos(\theta_1 - \theta_2)$. Using the transformation matrix

$$T = \begin{pmatrix} 1 & 0 & 1 & 0 \\ 0 & 1 & 0 & 1 \\ 1 & 0 & -1 & 0 \\ 0 & 1 & 0 & -1 \end{pmatrix},$$

which generalizes the matrix P given by (22) for (S2) we diagonalize the matrix M into two blocks after a similarity transformation:

$$T^{-1}MT = \begin{pmatrix} a+b & -a-b & 0 & 0 \\ -a-b & a+b & 0 & 0 \\ 0 & 0 & a+b & a-b \\ 0 & 0 & a-b & a+b \end{pmatrix}.$$

Note that the first block is given by a singular matrix, whereas the second block coincides with the Jacobian matrix $\mathcal{N}(\boldsymbol{\theta})$ given by (16).

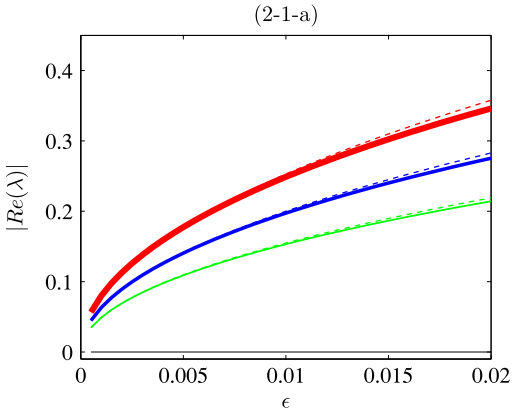

Fig. 13. The real parts of eigenvalues λ as functions of ϵ at $\gamma = 0.8$ for the branch (2-1-a) in comparison with the analytically approximated eigenvalues (dashed lines). The imaginary parts are identically zero, i.e., all three nonzero eigenvalue pairs are real.

The following list summarizes stability of the branches (2-1) and (2-2) among the solutions of the system (17), which corresponds to the particular symmetry (S2S) with $\gamma_1 = -\gamma_2 = \gamma$.

(2-1) For the solution with $\theta_2 = -\theta_1$ and $\sin(2\theta_1) = -\gamma$, we obtain $a = 1$ and $b = \cos(2\theta_1)$. Therefore, the matrix $\mathcal{M}$ has zero eigenvalue $\mu_1 = 0$ with eigenvector $(1, 1, 1, 1)^T$ and three simple nonzero eigenvalues $\mu_2 = 2$ with eigenvector $(-1, -1, 1, 1)^T$, $\mu_3 = 2\cos(2\theta_1)$ with eigenvector $(1, -1, -1, 1)^T$, and $\mu_4 = 2 + 2\cos(2\theta_1)$ with eigenvector $(-1, 1, -1, 1)^T$.

For $\epsilon > 0$, the spectral problem (24) has at least one pair of real eigenvalues λ near $\pm\sqrt{4\epsilon}$ so that the stationary solutions are spectrally unstable for both branches (2-1-a) and (2-1-b). The numerical results shown in Figs. 13 and 14 illustrate the validity of the first-order approximations for the eigenvalues of the spectral stability problem (24).

(2-2) For the solution with $\theta_2 = -\theta_1 \pm \pi$ and $\sin(2\theta_1) = \gamma$, we obtain $a = -1$ and $b = -\cos(2\theta_1)$. Therefore, the matrix $\mathcal{M}$ has zero eigenvalue $\mu_1 = 0$ with eigenvector $(1, 1, 1, 1)^T$ and three simple nonzero eigenvalues $\mu_2 = -2$, $\mu_3 = -2\cos(2\theta_1)$, and $\mu_4 = 2 + 2\cos(2\theta_1)$. These eigenvalues are opposite to those in the case (2-1), because the family (2-2) is related to the family (2-1) by Remark 2.2. Consequently, the stability analysis of the family (2-2) for $\epsilon > 0$ corresponds to the stability analysis of the family (2-1) for $\epsilon < 0$.

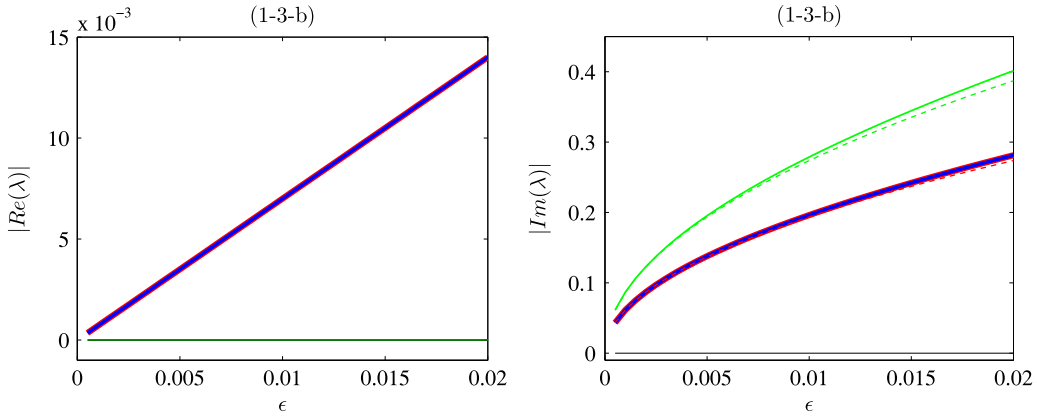

Fig. 12. The real (left) and imaginary (right) parts of eigenvalues λ as functions of ϵ at $\gamma = -0.7$ for the branch (1-3-b) in comparison with the analytically approximated eigenvalues (dashed lines). In the left panel, two thicker (red and blue) solid lines for nonzero eigenvalues as well as two thinner (black and green) solid lines for zero real parts are identical. Similarly, the two thicker (red and blue) solid lines for nonzero eigenvalues are identical in the right panel. These two sets of coincident lines correspond to the complex eigenvalue quartet which emerges in this case, destabilizing the soliton configuration. Splitting of the double imaginary eigenvalues is beyond the leading-order asymptotic theory. (For interpretation of the references to color in this figure legend, the reader is referred to the web version of this article.)

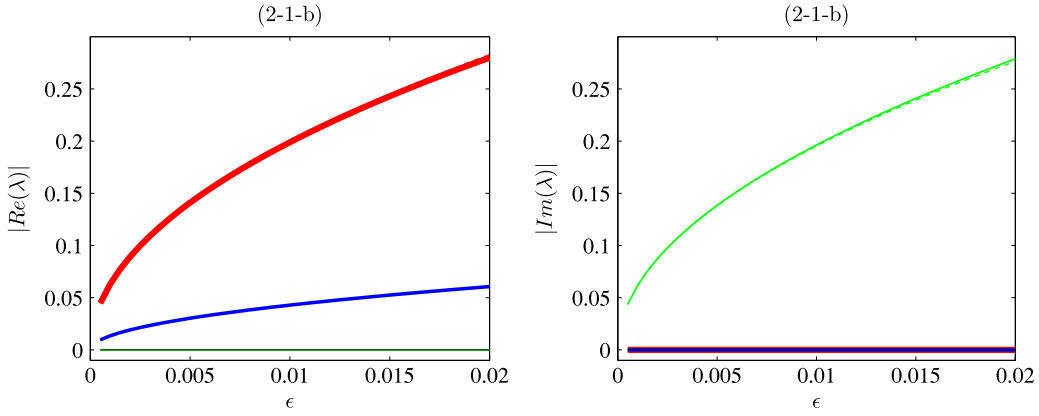

Fig. 14. The real and imaginary parts of eigenvalues λ as functions of ϵ at $\gamma = -0.3$ for the branch (2-1-b) in comparison with the analytically approximated eigenvalues (dashed lines). In the left panel two thinner (green and black) solid lines are zero while in the right panel three (red, blue and black) lines are zero. Here, two of the relevant eigenvalue pairs are found to be real, while the other is imaginary. In both panels, the solid lines and dashed lines look almost identical. (For interpretation of the references to color in this figure legend, the reader is referred to the web version of this article.)

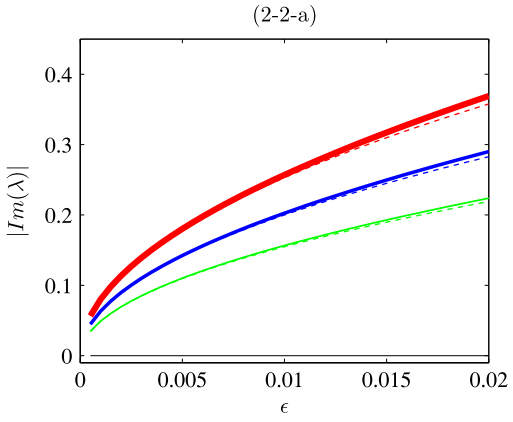

Fig. 15. The imaginary parts of eigenvalues λ as functions of ϵ at $\gamma = 0.8$ for the stable branch (2-2-a) in comparison with the analytically approximated eigenvalues (dashed lines). The real parts of the eigenvalues are identically zero.

For the branch (2-2-a), the spectral stability problem (24) with $\epsilon > 0$ has three pairs of simple purely imaginary eigenvalues λ near $\pm 2i\sqrt{\epsilon}$, $\pm 2i\sqrt{\epsilon\cos(2\theta_1)}$, and $\pm 2i\sqrt{\epsilon(1+\cos(2\theta_1))}$. Therefore, the stationary solution is spectrally stable at least for small values of $\epsilon > 0$. For the branch (2-2-b), the spectral stability problem (24) with $\epsilon > 0$ includes a pair of real eigenvalues near $\pm 2\sqrt{|\epsilon\cos(2\theta_1)|}$, which implies instability of the stationary solutions. The numerical results shown in Figs. 15 and 16 illustrate the validity of these predictions.

4.3. Summary on the stability in the elementary cell

Among all the irreducible branches of solutions examined in the elementary cell, we conclude

- all the vortex configurations (1-1) are spectrally unstable;
- most of the soliton configurations (1-3), (2-1) and (2-2-b) are spectrally unstable;
- the only stable soliton configuration is branch (2-2-a).

5. Stability of $\mathcal{PT}$-symmetric configurations in truncated lattice

Here we extend the spectral stability analysis of the $\mathcal{PT}$-symmetric configurations to the setting of the truncated square lattice. Persistence of these configurations in small parameter ϵ is obtained in Section 3.

Let n be an even number and consider the n-by-n square lattice, denoted by L_n. The domain is truncated symmetrically with zero boundary conditions. The $\mathcal{PT}$-symmetric solution $\{\phi_{j,k}\}_{(j,k)\in L_n}$ to the system (20) is supposed to satisfy the limiting configuration (21), where the central cell S is now placed at

$$S = \left\{\left(\frac{n}{2}, \frac{n}{2}\right), \left(\frac{n}{2}, \frac{n}{2}+1\right), \left(\frac{n}{2}+1, \frac{n}{2}\right), \left(\frac{n}{2}+1, \frac{n}{2}+1\right)\right\},$$

whereas the zero sites are located at $S^* := L_n \backslash S$. In addition to spectral stability of the $\mathcal{PT}$-symmetric solution, we also consider spectral stability of the zero equilibrium.

No matter whether the sites at S are excited or not, the spectral stability problem can be written in the form (24), where $\boldsymbol{\xi}$ now consists of blocks of $(v_{j,k}, w_{j,k})^T$, $\mathcal{G}$ consists of blocks of $\gamma_{j,k}\sigma_3$, and $\mathcal{H}$ consists of the blocks of

$$\mathcal{H}_{j,k} = \begin{pmatrix} 1-2|\phi_{j,k}|^2 & -(\phi_{j,k})^2 \\ -(\overline{\phi_{j,k}})^2 & 1-2|\phi_{j,k}|^2 \end{pmatrix} - \epsilon(s_{0,+1}+s_{0,-1}+s_{-1,0}+s_{+1,0})\begin{pmatrix} 1 & 0 \\ 0 & 1 \end{pmatrix}, \tag{38}$$

where $s_{l,m}$ stands for the shift operator such that $(s_{l,m}\phi)_{j,k} = \phi_{j+l,k+m}$.

5.1. Spectral stability of the zero equilibrium

Here we construct explicit solutions of the spectral stability problem (24) associated with the zero solution $\phi_{j,k} = 0$ for every $(j,k) \in L_n$. In this case, the spectral stability problem (24) is given by two uncoupled linear difference equations for $\{v_{j,k}\}_{(j,k)\in L_n}$ and $\{w_{j,k}\}_{(j,k)\in L_n}$. The linear difference equations for $\{v_{j,k}\}_{(j,k)\in L_n}$ are given by

$$(1+i\epsilon\gamma_{j,k})v_{j,k} - \epsilon(v_{j+1,k}+v_{j-1,k}+v_{j,k+1}+v_{j,k-1}) = i\lambda v_{j,k}, \quad (j,k)\in L_n, \tag{39}$$

whereas the linear difference equations for $\{w_{j,k}\}_{(j,k)\in L_n}$ are given by

$$(1-i\epsilon\gamma_{j,k})w_{j,k} - \epsilon(w_{j+1,k}+w_{j-1,k}+w_{j,k+1}+w_{j,k-1}) = -i\lambda w_{j,k}, \quad (j,k)\in L_n. \tag{40}$$

Since the values of $\gamma_{j,k}$ are anti-symmetric about the line or center of the $\mathcal{PT}$-symmetry, eigenvalues of (40) correspond to the negative of the eigenvalues of (39). Therefore, it is sufficient to consider eigenvalues of the spectral problem (39).

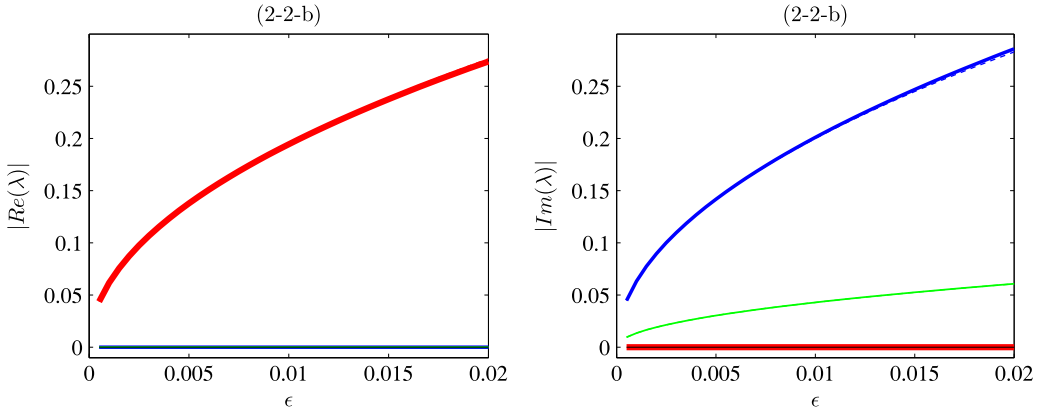

Fig. 16. The real parts of eigenvalues λ as functions of ϵ at $\gamma = 0.3$ for the branch (2-2-b) in comparison with the approximated eigenvalues (dashed lines). In the left panel three thinner (blue, green and black) solid lines are zero while in the right panel the thickest and thinnest (red and black) solid lines are zero. Here, one of the three eigenvalue pairs is found to be real, while the other two are imaginary. In both panels, the solid and dashed lines look almost identical. (For interpretation of the references to color in this figure legend, the reader is referred to the web version of this article.)

The $\mathcal{PT}$-symmetric configurations for the symmetries (S1S) and (S2S) correspond to the cases $\gamma_{j,k} = (-1)^{j+k}\gamma$ and $\gamma_{j,k} = (-1)^k\gamma$ for all $(j,k) \in L_n$, where $\gamma \in \mathbb{R}$. In the first case, we shall prove that the linear eigenvalue problem (39) includes complex eigenvalues λ with positive real parts for every $\gamma \neq 0$ such that the zero equilibrium is spectrally unstable for every $\gamma \neq 0$. In the second case, we shall prove that the linear eigenvalue problem (39) admits only purely imaginary eigenvalues λ if $|\gamma|$ is small such that the zero equilibrium is spectrally stable for small $|\gamma|$.

Lemma 5.1. *Let $\gamma_{j,k} = (-1)^{j+k}\gamma$ for all $(j,k) \in L_n$ with even n. Then, the linear eigenvalue problem (39) admits n^2 eigenvalues in the closed analytical form*

$$i\lambda = 1 \pm 2\epsilon\sqrt{\left[\cos\left(\frac{\pi l}{n+1}\right) \pm \cos\left(\frac{\pi m}{n+1}\right)\right]^2 - \frac{\gamma^2}{4}}, \quad 1 \le l, m \le \frac{n}{2}, \tag{41}$$

where the two plus/minus signs are independent from each other. Consequently, there are $n/2$ eigenvalues with $l = m$, for which $\mathrm{Re}(\lambda) = \epsilon|\gamma| > 0$ for every $\gamma \neq 0$.

Proof. In the case $\gamma_{j,k} = (-1)^{j+k}\gamma$, $(j,k) \in L_n$, we can use the linear difference equations (39) twice in order to close the system for the components $v_{j,k}$ with $(j,k) \in L_n$ such that $j + k =$ even. These components correspond to the values $\gamma_{j,k} = \gamma$. As a result, we obtain the extended linear difference equation

$$\left[(1-i\lambda)^2 + \epsilon^2\gamma^2\right] v_{j,k} = \epsilon^2\left[v_{j+2,k} + v_{j-2,k} + v_{j,k+2} + v_{j,k-2} + 4v_{j,k} + 2v_{j+1,k+1} + 2v_{j-1,k+1} + 2v_{j+1,k-1} + 2v_{j-1,k-1}\right], \quad (j,k) \in L_n,\ j+k = \text{even}. \tag{42}$$

The linear difference equations (42) have (j,k)-independent coefficients. Therefore, we can use the discrete Fourier transform to solve it explicitly. However, due to the constraints $j+k =$ even, we have two arrays of the corresponding variables:

$$V_{J,K} := v_{2J-1,2K-1}, \qquad U_{J,K} := v_{2J,2K}, \quad 1 \le J, K \le N,$$

where $N = n/2$. Therefore, we rewrite the linear difference equations (42) in the coupled form:

$$\left[(1-i\lambda)^2 + \epsilon^2\gamma^2\right] V_{J,K} = \epsilon^2\left[V_{J+1,K} + V_{J-1,K} + V_{J,K+1} + V_{J,K-1} + 2U_{J-1,K-1} + 2U_{J-1,K} + 2U_{J,K-1} + 2U_{J,K} + 4V_{J,K}\right] \tag{43}$$

and

$$\left[(1-i\lambda)^2 + \epsilon^2\gamma^2\right] U_{J,K} = \epsilon^2\left[U_{J+1,K} + U_{J-1,K} + U_{J,K+1} + U_{J,K-1} + 2V_{J+1,K+1} + 2V_{J+1,K} + 2V_{J,K+1} + 2V_{J,K} + 4U_{J,K}\right], \tag{44}$$

where $1 \le J, K \le N$. The linear system (43)–(44) is equipped with the boundary conditions

$$U_{0,K} = U_{J,0} = V_{N+1,K} = V_{J,N+1} = 0, \quad 1 \le J, K \le N. \tag{45}$$

Each of the Fourier harmonics $V_{J,K}, U_{J,K} \sim e^{i\theta J + i\varphi K}$ solves the linear system (43)–(44) with the characteristic equation in the form

$$\left[(1-i\lambda)^2 + \epsilon^2\gamma^2 - 2\epsilon^2(\cos\theta + \cos\varphi) - 4\epsilon^2\right]^2 = 4\epsilon^4(1+\cos\theta)(1+\cos\varphi). \tag{46}$$

Since the characteristic equation (46) is even in θ and φ, all four Fourier harmonics $V_{J,K}, U_{J,K} \sim e^{\pm i\theta J \pm i\varphi K}$ correspond to the same value of λ. Therefore, we construct a linear combination of the four Fourier harmonics to satisfy the first set of the boundary conditions (45):

$$U_{J,K} = \sin(\theta J)\sin(\varphi K), \quad 1 \le J, K \le N. \tag{47}$$

If follows from the original system (39) that the second set of the boundary conditions (45) for $V_{N+1,K}$ and $V_{J,N+1}$ is equivalent to the boundary conditions

$$U_{N+1,K} = -U_{N,K}, \qquad U_{J,N+1} = -U_{J,N}, \quad 1 \le J, K \le N. \tag{48}$$

These boundary conditions are satisfied independently by

$$\sin\left(\frac{(2N+1)\theta}{2}\right)\cos\left(\frac{\theta}{2}\right) = 0, \qquad \sin\left(\frac{(2N+1)\varphi}{2}\right)\cos\left(\frac{\varphi}{2}\right) = 0. \tag{49}$$

Therefore, the values of parameters θ and φ are discretized as follows:

$$\theta = \frac{2\pi l}{2N+1}, \qquad \varphi = \frac{2\pi m}{2N+1}, \quad 1 \le l, m \le N. \tag{50}$$

Extracting the first square root, we reduce the characteristic equation (46) to the form

$$(1-i\lambda)^2+\epsilon^2\gamma^2-4\epsilon^2\cos^2\frac{\theta}{2}-4\epsilon^2\cos^2\frac{\varphi}{2} = \pm 4\epsilon^2\cos\frac{\theta}{2}\cos\frac{\varphi}{2}. \tag{51}$$

Regrouping the terms and extracting the second square root, the characteristic equation (51) can now be written in the form (41). Note that we count all n^2 eigenvalues with two independent square roots. □

Lemma 5.2. *Let $\gamma_{j,k}=(-1)^k\gamma$ for all $(j,k)\in L_n$ with even n. Then, the linear eigenvalue problem (39) admits n^2 eigenvalues in the closed analytical form*

$$i\lambda = 1-2\epsilon\cos\left(\frac{\pi l}{n+1}\right)\pm 2\epsilon\sqrt{\cos^2\left(\frac{\pi m}{n+1}\right)-\frac{\gamma^2}{4}}, \quad 1\le l\le n,\ 1\le m\le\frac{n}{2}. \tag{52}$$

Consequently, $\mathrm{Re}(\lambda)=0$ *for every* $\gamma\in(-\gamma_n,\gamma_n)$, *where*

$$\gamma_n := 2\cos\left(\frac{\pi n}{2n+2}\right).$$

Proof. In the case $\gamma_{j,k}=(-1)^k\gamma$, $(j,k)\in L_n$, we can separate the variables of the linear difference equations (39) in the form

$$i\lambda = 1+\epsilon\left(\Lambda_x+\Lambda_y\right), \qquad v_{j,k}=x_jy_k, \quad (j,k)\in L_n, \tag{53}$$

where Λ_x is the eigenvalue of the spectral problem

$$\Lambda_x x_j = -(x_{j+1}+x_{j-1}), \quad 1\le j\le n, \tag{54}$$

and Λ_y is the eigenvalue of the spectral problem

$$\Lambda_y y_k = -(y_{k+1}+y_{k-1})+i(-1)^k\gamma y_k, \quad 1\le k\le n, \tag{55}$$

subject to the homogeneous Dirichlet end-point conditions. The first problem (54) is solved with the discrete sine Fourier transform

$$\Lambda_x = -2\cos\left(\frac{\pi l}{n+1}\right), \quad x_j=\sin\left(\frac{\pi lj}{n+1}\right), \quad 1\le l\le n. \tag{56}$$

The second problem (55) has been solved in [2] using the method similar to the proof of Lemma 5.1. For reader's convenience, we give a quick reconstruction of the solution here. Eliminating y_k for odd k and denoting $z_k=y_{2k}$ for $1\le k\le N$, where $N=n/2$, we obtain from (55) the linear difference equations with constant coefficients:

$$(\Lambda_y^2+\gamma^2)z_k = z_{k+1}+2z_k+z_{k-1}, \quad 1\le k\le N, \tag{57}$$

subject to the boundary conditions $z_0=0$ and $z_{N+1}=-z_N$. The spectral problem (57) is now solved with the discrete sine Fourier transform

$$\Lambda_y^2+\gamma^2 = 4\cos^2\left(\frac{\pi m}{2N+1}\right), \qquad z_k=\sin\left(\frac{2\pi mk}{2N+1}\right), \quad 1\le m\le N, \tag{58}$$

which satisfies both the boundary conditions $z_0=0$ and $z_{N+1}=-z_N$. Extracting square roots and substituting (56) and (58) into (53), we obtain n^2 eigenvalues of the linear eigenvalue problem (39) in the explicit form (52). □

5.2. Spectral stability of the $\mathcal{PT}$-symmetric solutions

At $\epsilon=0$, we have $|\phi_{j,k}^{(0)}|=1$ for $(j,k)\in S$ and $\phi_{j,k}^{(0)}=0$ for $(j,k)\in S^*$. The limiting operator $\mathcal{H}^{(0)}$ given by (38) for $\epsilon=0$ has two semi-simple eigenvalues $\mu=0$ and $\mu=-2$ of multiplicity four and a semi-simple eigenvalue $\mu=1$ of multiplicity $2n^2-8$. On the other hand, the spectral stability problem (24) for $\epsilon=0$ has the zero eigenvalue $\lambda=0$ of geometric multiplicity four and algebraic multiplicity eight and a pair of semi-simple eigenvalues $\lambda=\pm i$ of multiplicity n^2-4.

When ϵ is nonzero but small, the splitting of the zero eigenvalue $\lambda=0$ is the same as that on the elementary cell S if the splitting occurs in the first-order perturbation theory. However, unless $\gamma_{j,k}=0$ for all $(j,k)\in S^*$, the splitting of the semi-simple eigenvalues $\lambda=\pm i$ is non-trivial and can possibly lead to instability, as is shown in the analysis of [3].

In order to study the splitting of the semi-simple eigenvalues $\lambda=\pm i$ for small but nonzero ϵ, we expand $\boldsymbol{\xi}=\boldsymbol{\xi}^{(0)}+\epsilon\boldsymbol{\xi}^{(1)}+\mathcal{O}(\epsilon^2)$ and $\lambda=\lambda^{(0)}+\epsilon\lambda^{(1)}+\mathcal{O}(\epsilon^2)$ where $\lambda^{(0)}=\pm i$, and obtain the perturbation equations

$$\mathcal{H}^{(0)}\boldsymbol{\xi}^{(0)} = i\lambda^{(0)}\sigma\boldsymbol{\xi}^{(0)}, \tag{59}$$

and

$$(\mathcal{H}^{(1)}+i\mathcal{G})\boldsymbol{\xi}^{(0)}+\mathcal{H}^{(0)}\boldsymbol{\xi}^{(1)} = i\lambda^{(0)}\sigma\boldsymbol{\xi}^{(1)}+i\lambda^{(1)}\sigma\boldsymbol{\xi}^{(0)}. \tag{60}$$

Since $i\lambda^{(0)}\in\mathbb{R}$, the operator $(\mathcal{H}^{(0)}-i\lambda^{(0)}\sigma)$ is self-adjoint, and we denote the spanning set for $\ker(\mathcal{H}^{(0)}-i\lambda^{(0)}\sigma)$ by $\{\boldsymbol{\psi}_{j,k}\}_{(j,k)\in S^*}$. Then, $\boldsymbol{\xi}^{(0)}=\sum_{(j,k)\in S^*}c_{j,k}\boldsymbol{\psi}_{j,k}$ satisfies (59). Projection of (60) to $\ker(\mathcal{H}^{(0)}-i\lambda^{(0)}\sigma)$ yields the matrix eigenvalue problem

$$i\lambda^{(1)}D\boldsymbol{c} = K\boldsymbol{c}, \tag{61}$$

where

$$D_{\mathcal{P}(j_1,k_1),\mathcal{P}(j_2,k_2)} = \langle\boldsymbol{\psi}_{j_1,k_1},\sigma\boldsymbol{\psi}_{j_2,k_2}\rangle,$$
$$K_{\mathcal{P}(j_1,k_1),\mathcal{P}(j_2,k_2)} = \langle\boldsymbol{\psi}_{j_1,k_1},(\mathcal{H}^{(1)}+i\mathcal{G})\boldsymbol{\psi}_{j_2,k_2}\rangle,$$

for $(j_1,k_1),(j_2,k_2)\in S^*$. The bijective mapping $\mathcal{P}: S^*\to\{1,2,\ldots,n^2-4\}$ is defined by

$$\mathcal{P}(j,k)=\begin{cases}(j-1)n+k, \\ \quad (j-1)n+k<\left(\frac{n}{2}-1\right)n+\frac{n}{2} \\ (j-1)n+k-2, \\ \quad \left(\frac{n}{2}-1\right)n+\frac{n}{2}+1<(j-1)n+k<\frac{n^2}{2}+\frac{n}{2} \\ (j-1)n+k-4, \\ \quad (j-1)n+k>\frac{n^2}{2}+\frac{n}{2}+1\end{cases} \tag{62}$$

assuming that the lattice L_n is traversed in the order

$$(1,1),(1,2),\ldots,(1,n),(2,1),(2,2),\ldots,(2,n),\ldots,$$
$$(n,1),(n,2),\ldots,(n,n).$$

For $i\lambda^{(0)}=1$, the eigenvector $\boldsymbol{\psi}_{j,k}$ has the only nonzero block $(1,0)^T$ at $\mathcal{P}(j,k)$th position which corresponds to position (j,k) on the lattice. Therefore, we have $D=I_{n^2-4}$ and

$$K_{\mathcal{P}(j_1,k_1),\mathcal{P}(j_2,k_2)}=\begin{cases}i\gamma_{j_1,k_1}, & (j_1,k_1)=(j_2,k_2)\\ -1, & |j_1-j_2|+|k_1-k_2|=1\\ 0, & \text{otherwise.}\end{cases} \tag{63}$$

For $i\lambda^{(0)} = -1$, the eigenvector $\boldsymbol{\psi}_{j,k}$ has the only nonzero block $(0, 1)^T$ at $\mathcal{P}(j, k)$th position, then $D = -I_{n^2-4}$ and K is the complex conjugate of K given by (63). Since the values of $\gamma_{j,k}$ are anti-symmetric about the line or center of the $\mathcal{PT}$-symmetry, the eigenvalues of the reduced eigenvalue problem (61) for $i\lambda^{(0)} = -1$ are negative of those for $i\lambda^{(0)} = 1$.

The $\mathcal{PT}$-symmetric configurations for the symmetries (S1S) and (S2S) correspond to the cases $\gamma_{j,k} = (-1)^{j+k}\gamma$ and $\gamma_{j,k} = (-1)^k\gamma$ for all $(j, k) \in L_n$, where $\gamma \in \mathbb{R}$. In the first case, we shall prove that the eigenvalues $\lambda^{(1)}$ of the reduced eigenvalue problem (61) include at least one pair of real eigenvalues for every $\gamma \neq 0$. In the second case, we shall show numerically that the eigenvalues $\lambda^{(1)}$ of the reduced eigenvalue problem (61) remain purely imaginary for sufficiently small $\gamma \neq 0$.

Lemma 5.3. *Let $\gamma_{j,k} = (-1)^{j+k}\gamma$ for all $(j, k) \in L_n$ and let K be given by (63). If we define $A = \mathrm{Re}(K)$ and $B = \mathrm{Im}(K|_{\gamma=1})$ then A and B anti-commute, i.e. $AB = -BA$.*

Proof. By inspecting the definition of matrices in (63) with $\gamma_{j,k} = (-1)^{j+k}\gamma$ for all $(j, k) \in L_n$, we observe that A is symmetric, B is diagonal, and $B^2 = I_{n^2-4}$. In calculating AB and BA, the ith row of A is multiplied by ith entry in the diagonal of B, while the ith column of A is multiplied by ith entry in the diagonal of B. In the lattice $S^* \subset L_n$, each site at (j_1, k_1) with $\gamma_{j_1,k_1} = \gamma$ is surrounded by sites (j_2, k_2) with $\gamma_{j_2,k_2} = -\gamma$ and vice versa, so that each nonzero entry in A must sit in a position $(\mathcal{P}(j_1, k_1), \mathcal{P}(j_2, k_2))$, where $\gamma_{j_1,k_1} = -\gamma_{j_2,k_2}$. Hence, we verify that $AB = -BA$. □

Lemma 5.4. *Under the assumptions of Lemma 5.3, A has a zero eigenvalue of multiplicity at least $n - 2$.*

Proof. At first, we assume the lattice is L_n and consider the spectral problem $\tilde{A}\boldsymbol{u} = \lambda\boldsymbol{u}$, where

$$\tilde{A}_{(j_1-1)n+k_1,(j_2-1)n+k_2} = \begin{cases} -1, & |j_1 - j_2| + |k_1 - k_2| = 1 \\ 0, & \text{otherwise} \end{cases} \tag{65}$$

for $(j_{1,2}, k_{1,2}) \in L_n$. The spectral problem represents the linear difference equations with constant coefficients:

$$-u_{j,k+1} - u_{j,k-1} - u_{j+1,k} - u_{j-1,k} = \lambda u_{j,k}, \quad (j, k) \in L_n, \tag{66}$$

which are closed with the Dirichlet end-point conditions. Similar to Lemmas 5.1 and 5.2, this spectral problem can be solved with the double discrete Fourier transform, from which we obtain the eigenvalues

$$\lambda(l, m) = -2\cos\left(\frac{l\pi}{n+1}\right) - 2\cos\left(\frac{m\pi}{n+1}\right), \quad 1 \le l, m \le n$$

and the eigenvectors

$$u_{j,k}(l, m) = \sin\left(\frac{jl\pi}{n+1}\right)\sin\left(\frac{km\pi}{n+1}\right), \quad 1 \le l, m \le n.$$

Thus, the spectral problem (66) has n^2 eigenvalues, among which n eigenvalues are zero and they correspond to $l + m = n + 1$.

Now, the spectral problem $A\boldsymbol{v} = \lambda\boldsymbol{v}$ is actually posed in $S^* := L_n \backslash S$, which is different from the spectral problem (66) by adding four constraints $u_{j,k} = 0$ for $(j, k) \in S$. A linear span of n linearly independent eigenvectors for the zero eigenvalue of multiplicity n satisfies the four constraints at the subspace, whose dimension is at least $n - 4$. In fact, it can be directly checked that

$$\begin{aligned} u_{j,k}(l, n+1-l) &= (-1)^{k+1}\sin\left(\frac{jl\pi}{n+1}\right)\sin\left(\frac{kl\pi}{n+1}\right) \\ &= -u_{n+1-j,n+1-k}(l, n+1-l) \end{aligned}$$

for any $1 \le j, k, l \le n$. In particular, we notice that the $n \times 4$ matrix consisting of $u_{j,k}(l, n + 1 - l)$, where $1 \le l \le n$ and $(j, k) \in S$, is of rank 2. Therefore, linear combinations of $\{\boldsymbol{u}(l, n + 1 - l)\}_{l=1}^n$ that satisfy the constraints $u(j, k) = 0$ for $(j, k) \in S$ form a subspace of dimension $n - 2$ for $\boldsymbol{v}$ and the lemma is proved. □

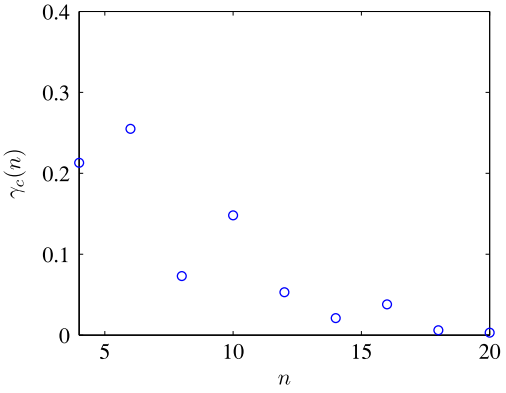

Fig. 17. The threshold γ_c versus even n for existence of stable eigenvalues in the reduced eigenvalue problem (61) with $\gamma_{j,k} = (-1)^k\gamma$ for all $(j, k) \in L_n$. Accounting also for numerical errors, here we call a numerically computed eigenvalue stable if the absolute value of its real part is less than 10^{-7}.

Lemma 5.5. *Let $\gamma_{j,k} = (-1)^{j+k}\gamma$ for all $(j, k) \in L_n$, $D = I_{n^2-4}$, and K be given by (63). Then, there is at least one pair of real eigenvalues $\lambda^{(1)}$ of the reduced eigenvalue problem (61) for every $\gamma \neq 0$.*

Proof. By Lemma 5.3, we can write $K = A + i\gamma B$ where $B^2 = I_{n^2-4}$ and $AB = -BA$. Squaring the reduced eigenvalue problem (61), we obtain

$$K^2\boldsymbol{c} = \left(A^2 - \gamma^2 I_{n^2-4}\right)\boldsymbol{c} = -(\lambda^{(1)})^2\boldsymbol{c}.$$

Since A is symmetric, eigenvalues $\lambda^{(1)}$ are all purely imaginary for $\gamma = 0$. Nonzero eigenvalues $\lambda^{(1)}$ remain nonzero and purely imaginary for sufficiently small $\gamma \neq 0$, since K^2 is symmetric and real. On the other hand, by Lemma 5.4, A always has a zero eigenvalue ($n \ge 4$), hence K^2 has a negative eigenvalue $-\gamma^2$, which corresponds to a pair of real eigenvalues $\lambda^{(1)} = \pm\gamma$. □

Coming back to the branches (1-1), (1-2), and (1-3) of the $\mathcal{PT}$-symmetric configurations (S1S) studied in Section 2.1, they correspond to the case $\gamma_{j,k} = (-1)^{j+k}\gamma$ for all $(j, k) \in L_n$. By Lemma 5.5, the reduced eigenvalue problem (61) has at least one pair of real eigenvalues $\lambda^{(1)}$. Therefore, all $\mathcal{PT}$-symmetric configurations are unstable on the truncated square lattice L_n because of the sites in the set S^*. In addition, all the configurations are also unstable because of the sites in the central cell S, as explained in Section 4.1. Note that the instability on the set S^* is originated from the instability of the zero equilibrium on L_n prescribed by Lemma 5.1.

For the branches (2-1) and (2-2) of the $\mathcal{PT}$-symmetric configurations (S2S) studied in Section 2.2, they correspond to $\gamma_{j,k} = (-1)^k\gamma$ for all $(j, k) \in L_n$. We have checked numerically for all values of n up to $n = 20$ that the reduced eigenvalue problem (61) has all eigenvalues $\lambda^{(1)}$ on the imaginary axis, at least for small values of γ. Therefore, the stability of the zero equilibrium prescribed by Lemma 5.2 on L_n persists on the set S^*, although we are not able to show this analytically.

Let $\gamma_c(n)$ be the largest value of $|\gamma|$, for which the eigenvalues of K are purely real. Fig. 17 shows how γ_n changes with respect to even n from numerical computations. It is seen from the figure that $\gamma_c(n)$ decreases towards 0 as n grows. The latter property agrees with the analytical predictions in [24] for unbounded $\mathcal{PT}$-symmetric lattices with spatially extended gains and losses.

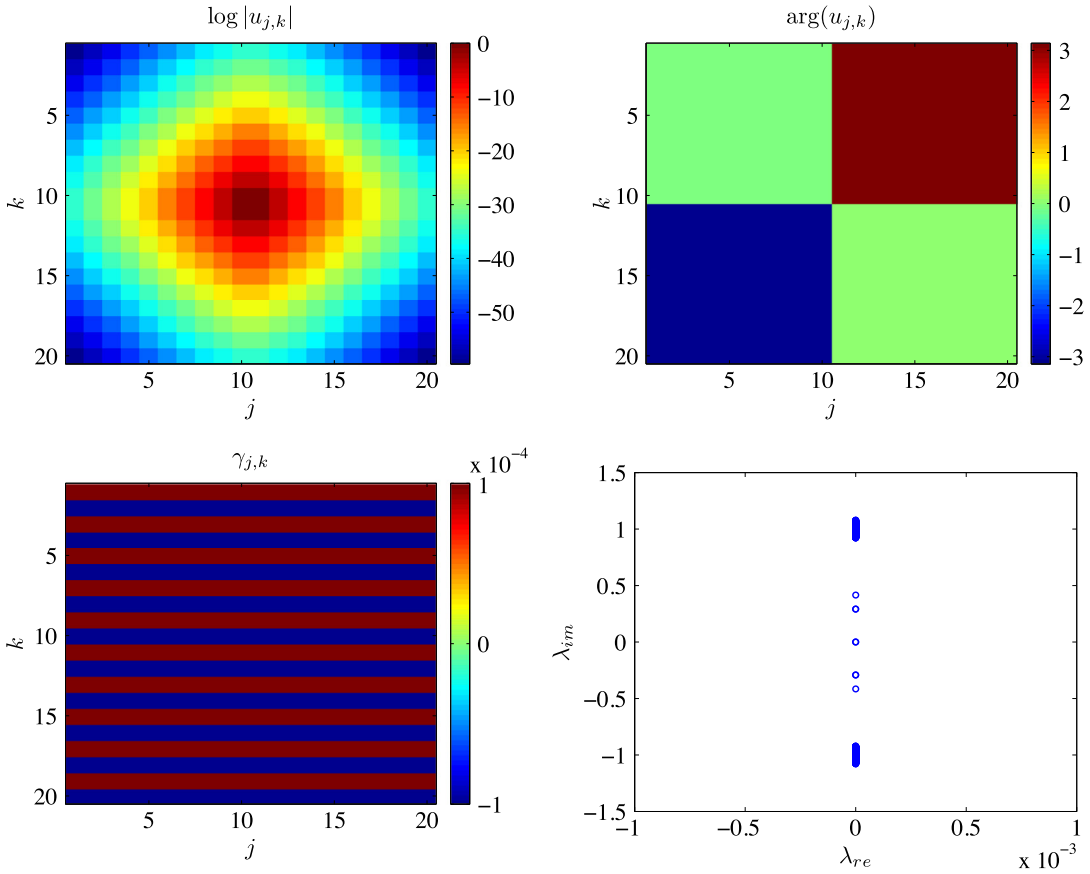

Fig. 18. An example of the branch (2-2-a) on the 20-by-20 square lattice with $\gamma_1 = -\gamma_2 = 0.0001 < \gamma_c(20) \approx 0.0003$ and $\epsilon = 0.02$. In the bottom right panel, we see eigenvalues λ of the spectral problem (24) are all on the imaginary axis, implying spectral stability of the stationary solution.

Besides the eigenvalue computations on the sites of S^*, one needs to add eigenvalue computations on the sites of S performed in Section 4.2. It follows from the results reported there that only the branch (2-2-a) is thus potentially stable, see Fig. 15. The branch of $\mathcal{PT}$-symmetric configurations remains stable on the extended square lattice L_n, provided $|\gamma| < \gamma_c(n)$.

In Fig. 18, we give an example of the stable $\mathcal{PT}$-symmetric solution on the 20-by-20 square lattice that continues from the branch (2-2-a) on the elementary cell S. When $\epsilon = 0$, the phases of the solution on S in (2-2-a) are $\{\theta_1, \pi - \theta_1, -\theta_1, \theta_1 - \pi\}$, where $\theta_1 = \frac{1}{2}\arcsin(\gamma)$, representing a discrete soliton in the form of an anti-symmetric (sometimes, called twisted) localized mode [16] if $\gamma = 0$. When $\epsilon = 0.02$ is small, we can observe on Fig. 18 that the solution is still close to the limiting solution at $\epsilon = 0$ in terms of amplitude and phase. Besides, the spectrum in the bottom right panel of Fig. 18 verifies our expectation about its spectral stability, bearing eigenvalues solely on the imaginary axis.

Finally, Fig. 19 provides some prototypical examples of the numerical evolution of the branches (1-1-a) and (2-1-a), which correspond to the $\mathcal{PT}$-symmetric configurations of Figs. 3 and 6. Both configurations are unstable, therefore, the figure illustrates the development of these instabilities. In the (1-1-a) example (top panels), the amplitudes of sites on (11, 11) and (10, 10) increase rapidly but those on (10, 11) and (11, 10) decrease. In the (2-1-a) example (bottom panels), the situation is reversed and sites on (11, 11) and (10, 11) grow rapidly while sites on (10, 10) and (11, 10) gradually decay. Both of these time evolutions are also intuitive, as the growth reflects the dynamics of the central sites bearing gain, while the decay reflects that of the ones bearing loss.

5.3. Summary on the stability results in truncated lattice

We examined the spectral stability of the solutions obtained in Section 3 in the truncated lattice. We notice that the splitting of the zero eigenvalues (corresponding to the sites in the center cell S) is the same as that in the single cell (shown in Section 4), up to $\mathcal{O}(\epsilon)$. On the other hand, the splitting of the eigenvalues $\lambda = \pm i$ (corresponding to the sites in S^*) is found to be related to the stability of the zero equilibrium on L_n. To be more specific,

- For the symmetry (S1S) with $\gamma_{j,k} = \gamma(-1)^{j+k}$, the splitting of the eigenvalues $\lambda = \pm i$ brings an eigenvalue pair with nonzero real parts and thus leads to spectral instability of all $\mathcal{PT}$-symmetric configurations with $\gamma \neq 0$.
- For the symmetry (S2S) with $\gamma_{j,k} = \gamma(-1)^k$, the eigenvalues remain on the imaginary axis if $|\gamma|$ is sufficiently small. As a result, the branch (2-2-a) of the $\mathcal{PT}$-symmetric configurations, which is spectrally stable on the four sites in S, remains spectrally stable on L_n for small $\gamma \neq 0$.

6. Conclusion

In the present work, we have provided a systematic perspective on discrete soliton and vortex configurations in the two-dimensional square lattices bearing $\mathcal{PT}$-symmetry. Both the existence and the stability features of the $\mathcal{PT}$-symmetric stationary states were elucidated in the vicinity of a suitable anti-continuum limit, which corresponds to the large propagation constant in optics. Interestingly, while discrete vortex solutions were identified, it was never possible to stabilize the $\mathcal{PT}$-symmetric vortex configurations in the square lattices considered herein. On

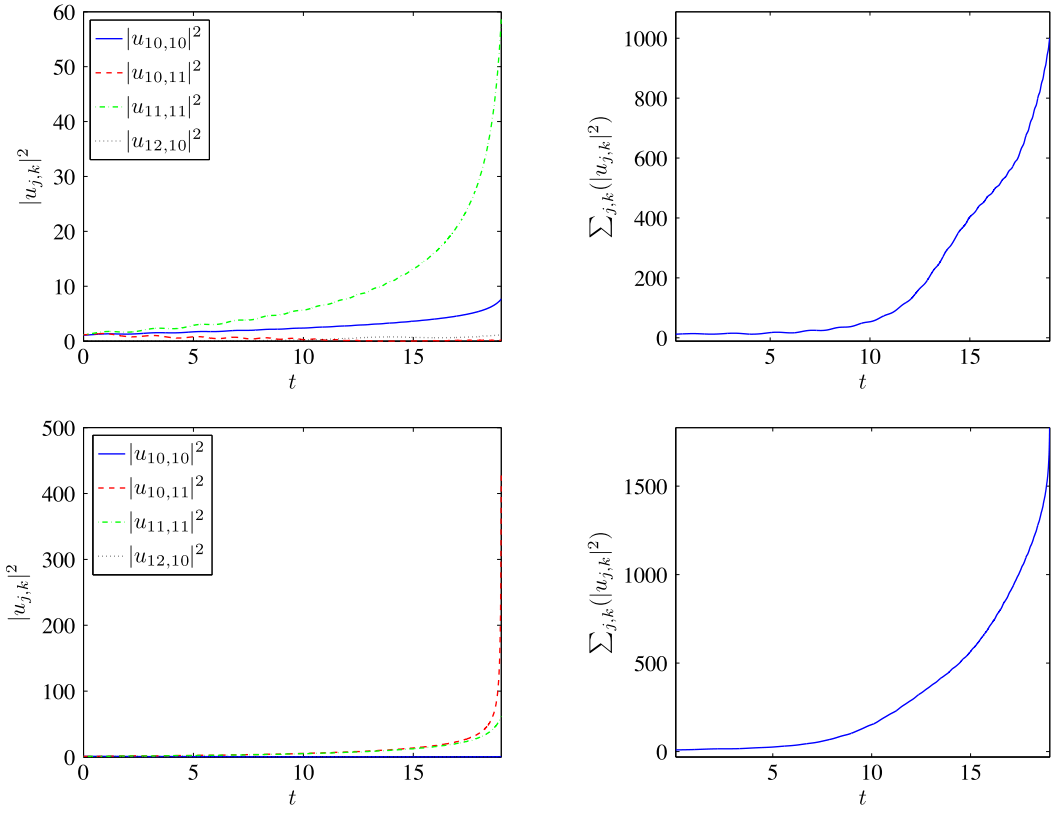

Fig. 19. The top panels show an example of the dynamics of the branch (1-1-a) on the 20-by-20 square lattice with $\gamma_1 = -\gamma_2 = 0.7$ and $\epsilon = 0.1$. The bottom panels show similar dynamics for the branch (2-1-a) with $\gamma_1 = -\gamma_2 = 0.8$ and $\epsilon = 0.1$. In the right column, we plot the total density on the 20×20 lattice which grows rapidly in both examples, as a result of instability.

the other hand, although stationary states extending discrete soliton configurations were found generally to be also unstable, we found one branch of potentially stable $\mathcal{PT}$-symmetric stationary states, at least for sufficiently small values of γ.

This work paves the way for numerous additional explorations. For instance, it may be relevant to extend the considerations of the square lattice to those of hexagonal or honeycomb lattices. Prototypical configurations in the $\mathcal{PT}$-symmetric settings have been explored in [14]. Such a study of non-square lattices may be of particular interest given that vortex states may manifest unexpected stability features in such lattices in the absence of gain and loss. One such example is that for focusing nonlinearities higher charge vortices are more robust than the lower charge ones [25]. In these lattices (as well as in the square lattice), it may also be relevant to explore systematic numerical continuations over the gain–loss parameter γ for fixed values of ϵ, since $\gamma = 0$ refers to the Hamiltonian case, where stable vortex solutions are quite common, see, e.g. [16,26].

Another relevant possibility is to extend the present consideration to a dimer lattice model, similarly to what was considered e.g. in [13]. The numerical considerations of [13] suggest that vortices may be stable in suitable parametric intervals in such a setting.

Lastly, it may be of interest to extend the present considerations also to three-dimensional settings, generalizing analysis of the corresponding Hamiltonian model of [23] (including cubes and diamonds) and exploring their stability properties.

Acknowledgments

P.G.K. gratefully acknowledges the support of NSF DMS-1312856, as well as the ERC under FP7, Marie Curie Actions, People, International Research Staff Exchange Scheme (IRSES-605096). The work of D.P. is supported by the Ministry of Education and Science of Russian Federation (the base part of the state task No. 2014/133).

References

[1] P.G. Kevrekidis, D.E. Pelinovsky, D.Y. Tyugin, Nonlinear dynamics in PT-symmetric lattices, J. Phys. A 46 (2013) 365201. 17 pages.
[2] P.G. Kevrekidis, D.E. Pelinovsky, D.Y. Tyugin, Nonlinear stationary states in PT-symmetric lattices, SIAM J. Appl. Dyn. Syst. 12 (2013) 1210–1236.
[3] D.E. Pelinovsky, D.A. Zezyulin, V.V. Konotop, Nonlinear modes in a generalized PT-symmetric discrete nonlinear Schrodinger equation, J. Phys. A 47 (2014) 085204. 20pp.
[4] S.V. Suchkov, B.A. Malomed, S.V. Dmitriev, Y.S. Kivshar, Solitons in a chain of parity-time-invariant dimers, Phys. Rev. E 84 (2011) 046609–8.
[5] S.V. Suchkov, A.A. Sukhorukov, J. Huang, S.V. Dmitriev, C. Lee, Yu. S. Kivshar, Nonlinear switching and solitons in PT-symmetric photonic systems, Laser Photon. Rev. 10 (2) (2016) 177–213.
[6] M. Wimmer, A. Regensburger, M.-A. Miri, C. Bersch, D.N. Christodoulides, U. Peschel, Observation of optical solitons in PT-symmetric lattices, Nature Commun. 6 (2014) 7782.
[7] Z.H. Musslimani, K.G. Makris, R. El Ganainy, D.N. Christodoulides, Optical solitons in PT periodic potentials, Phys. Rev. Lett. 100 (2008) 030402–4.
[8] Z.H. Musslimani, K.G. Makris, R. El Ganainy, D.N. Christodoulides, Analytical solutions to a class of nonlinear Schrodinger equations with PT-like potentials, J. Phys. A 41 (2008) 244019–12.
[9] Y.V. Kartashov, Vector solitons in parity-time-symmetric lattices, Opt. Lett. 38 (2013) 2600–2603.
[10] J. Yang, Partially PT symmetric optical potentials with all-real spectra and soliton families in multidimensions, Opt. Lett. 39 (2014) 1133–1136.
[11] X. Zhu, H. Wang, H.G. Li, W. He, Y.J. He, Two-dimensional multipeak gap solitons supported by parity time-symmetric periodic potentials, Opt. Lett. 38 (2013) 2723–2725.
[12] Y.V. Kartashov, V.V. Konotop, L. Torner, Topological states in partially-PT-symmetric azimuthal potentials, Phys. Rev. Lett. 115 (2015) 193902.
[13] Z.P. Chen, J.F. Liu, S.H. Fu, Y.Y. Li, B.A. Malomed, Discrete solitons and vortices on two-dimensional lattices of PT-symmetric couplers, Opt. Express 22 (2014) 29679–29692.
[14] D. Leykam, V.V. Konotop, A.S. Desyatnikov, Discrete vortex solitons and parity time symmetry, Opt. Lett. 38 (2013) 371–373.
[15] K. Li, P.G. Kevrekidis, B.A. Malomed, U. Guenther, Nonlinear $\mathcal{PT}$-symmetric plaquettes, J. Phys. A. 45 (2012) 444021.

[16] P.G. Kevrekidis, Discrete Nonlinear Schrodinger Equation: Mathematical Analysis, Numerical Computations and Physical Perspectives, Springer-Verlag, Berlin, 2009.
[17] F. Lederer, G.I. Stegeman, D.N. Christodoulides, G. Assanto, M. Segev, Y. Silberberg, Discrete solitons in optics, Phys. Rep. 463 (2008) 1–126.
[18] C. Rüter, K.G. Makris, R. El-Ganainy, D.N. Christodoulides, M. Segev, D. Kip, Observation of parity-time symmetry in optics, Nat. Phys. 6 (2010) 192–195.
[19] V.V. Konotop, D.E. Pelinovsky, D.A. Zezyulin, Discrete solitons in PT-symmetric lattices, Eur. Phys. Lett. 100 (2012) 56006. 6 pages.
[20] R.S. MacKay, S. Aubry, Proof of existence of breathers for time-reversible or Hamiltonian networks of weakly coupled oscillators, Nonlinearity 7 (6) (1994) 1623.
[21] D.E. Pelinovsky, P.G. Kevrekidis, D. Frantzeskakis, Persistence and stability of discrete vortices in nonlinear Schrodinger lattices, Physica D 212 (2005) 20–53.
[22] P.G. Kevrekidis, D.E. Pelinovsky, Discrete vector on-site vortices, Proc. R. Soc. Lond. Ser. A Math. Phys. Eng. Sci. 462 (2006) 2671–2694.
[23] M. Lukas, D. Pelinovsky, P.G. Kevrekidis, Lyapunov-Schmidt reduction algorithm for three-dimensional discrete vortices, Physica D 237 (2008) 339–350.
[24] D.E. Pelinovsky, P.G. Kevrekidis, D.J. Frantzeskakis, PT-symmetric Lattices with extended gain/loss are generically unstable, Eur. Phys. Lett. 101 (2013) 11002. 6 pages.
[25] B. Terhalle, T. Richter, K.J.H. Law, D. Göries, P. Rose, T.J. Alexander, P.G. Kevrekidis, A.S. Desyatnikov, W. Krolikowski, F. Kaiser, C. Denz, Yu.S. Kivshar, Observation of double-charge discrete vortex solitons in hexagonal photonic lattices, Phys. Rev. A 79 (2009) 043821.
[26] B.A. Malomed, P.G. Kevrekidis, Discrete vortex solitons, Phys. Rev. E 64 (2001) 026601.